Available online at www.sciencedirect.com

SCIENCE DIRECT

Cement and Concrete Research 36 (2006) 209 – 226

Cement and Concrete Research

# Thermodynamic modelling of the hydration of Portland cement

Barbara Lothenbach*, Frank Winnefeld

*Empa, Laboratory for Concrete and Construction Chemistry, Überlandstrasse 129, 8600 Dübendorf, Switzerland*

Received 11 March 2005; accepted 11 March 2005

**Abstract**

A thermodynamic model is developed and applied to calculate the composition of the pore solution and the hydrate assemblage during the hydration of an OPC. The calculated hydration rates of the individual clinker phases are used as time dependent input. The modelled data compare well with the measured composition of pore solutions gained from OPC as well as with TGA and semi-quantitative XRD data. The thermodynamic calculations indicate that in the presence of small amounts of calcite typically included in OPC cements, C-S-H, portlandite, ettringite and calcium monocarbonates are the main hydration products. The thermodynamic model presented in this paper helps to understand the interactions between the different components and the environment and to predict the influence of changes in cement composition on the hydrate assemblage.


*Keywords:* Thermodynamic calculations; Pore solution; Hydration products; Hydration; Modeling

## 1. Introduction

The principal constituents of ordinary Portland cement (OPC) are calcium silicates ($Ca_3SiO_5$ and $Ca_2SiO_4$), aluminate ($Ca_3Al_2O_6$), and ferrite ($Ca_4(Al_xFe_{1-x})_4O_{10}$) which are abbreviated to $C_3S$[1], $C_2S$, $C_3A$, and $C_4AF$. A number of other minerals such as calcium sulphates (present as gypsum, anhydrite and/or hemihydrate), calcite, calcium oxide, magnesium oxide, Na- and K-sulphates are usually also present. These constituents react with water to form various hydration products such as C-S-H (calcium silicate hydrate), portlandite, ettringite, calcium monosulphoaluminate or calcium monocarboaluminate.

The composition and development of the aqueous phase during cement hydration gives an important insight into the chemical processes and the interactions between liquid and solid phases, which control the setting and hardening of cements. The modelling of these interactions between solid and liquid phase in cements using geochemical speciation codes can be the basis for the chemical understanding of these processes and of the factors influencing them. In addition, adequate thermodynamic models allow easy and fast parameter variations and make it possible to predict the composition of hydrate assemblages under different conditions and to extrapolate it to longer time scales.

Several thermodynamic cement models [1–7] have been developed and applied to cementitious systems in order to predict the long-term behaviour as envisaged in many countries for the disposal of low and intermediate level radioactive waste. Rothstein et al. [8] applied thermodynamic calculations to obtain a better understanding of the changes in fresh cement systems and compared the measured compositions of pore solutions with the calculated saturation indexes of different solids (portlandite, gypsum, ettringite, calcium monosulphoaluminate and C-S-H phase). In this paper the established method of using thermodynamic modelling to calculate saturation indices in cementitious pore solutions is taken one step further by incorporating a simple model for the rate of consumption of cement minerals, so that the evolution of the solid phase assemblage and the pore solution can be predicted. The results of these model calculations are compared with

* Corresponding author. Tel.: +41 1 8234788; fax: +41 1 8234035.
*E-mail address:* barbara.lothenbach@empa.ch (B. Lothenbach).

[1] Idealized formulas, minor components might be present up to several percent. Key to abbreviations: A=$Al_2O_3$; C=CaO; F=$Fe_2O_3$; H=$H_2O$; S=$SiO_2$; C-S-H (non-stoichiometric) calcium silicate hydrate.

0008-8846/$ - see front matter © 2005 Elsevier Ltd. All rights reserved.
doi:10.1016/j.cemconres.2005.03.001

experimentally determined concentrations in the pore solution as well as with semi-quantitative XRD and TGA data obtained during the first year of the hydration of OPC.

## 2. Materials and methods

All experiments were carried out using an ordinary Portland cement (OPC), CEM I 42.5 N, at 20 °C. The composition of the cement and the calculated amount of the clinker phases in the unhydrated cement are compiled in Table 1. The distribution of alkali between sulphates and oxides is calculated using the measured concentration of "easily soluble" alkalis in bi-distilled water at a solid/water ratio of 0.1 after an equilibration time of 5 min. These easily soluble alkalis are assumed to correspond to the alkali sulphates present in the clinker, while the remaining K, Na, Mg and S are assumed to be present as minor constituents in solid solution with the major clinker phases [9,10] (cf. Table 2).

Cement pastes were prepared with a w/c of 0.5 by adding cement to distilled water. For the experiments with fresh pastes (up to 7 h), small samples of ~100 g were prepared, cured in the glove box under $N_2$-atmosphere and the pore solution was collected by vacuum filtration using 0.45 μm filter. For longer hydration times, larger samples consisting of 1 kg cement and 0.5 kg water were mixed for 3 min in a Hobart mixer. The pastes were cast in 0.5 l PE-bottles, sealed and stored under controlled conditions at 20 °C. Pore fluids of the hardened samples were extracted using the steel die method using pressures up to 250 N/mm$^2$; the solutions were filtered immediately (0.45 μm).

Table 1
Composition of the OPC used (CEM I 42.5N)

| Chemical analysis | | Normative phase composition[a] | | |
|---|---|---|---|---|
| | g/100 g | | g/100 g | mmol/100 g |
| $SiO_2$ | 19.7 | alite | 55 | 241 |
| $Al_2O_3$ | 4.7 | belite | 15 | 87 |
| $Fe_2O_3$ | 2.67 | aluminate | 7.9 | 29 |
| CaO | 63.2 | ferrite | 8.1 | 17 |
| MgO | 1.85 | CaO | 0.46 | 8.2 |
| SrO | 0.07 | $CaCO_3$ | 4.4 | 44 |
| $K_2O$ | 1.12 | $CaSO_4$[b] | 4.2 | 31 |
| $Na_2O$ | 0.08 | $K_2SO_4$[c] | 1.6 | 9.2 |
| CaO (free) | 0.46 | $Na_2SO_4$[c] | 0.096 | 0.67 |
| $CO_2$ | 1.93 | SrO | 0.07 | 0.68 |
| $SO_3$ | 3.35 | $K_2O$[d] | 0.26 | 2.7 |
| *readily soluble alkalis*[c] | | $Na_2O$[d] | 0.04 | 0.6 |
| $K_2O$ | 0.86 (77% of total K) | MgO[d] | 1.9 | 46 |
| $Na_2O$ | 0.042 (52% of total Na) | $SO_3$[d] | 0.12 | 1.4 |

Blaine surface area: 300 m$^2$/kg.
[a] Calculated from the chemical analysis.
[b] Present as anhydrite (2.5 g/100 g), hemihydrate (0.5 g/100 g) and gypsum (1.5 g/100 g).
[c] Readily soluble alkalis were calculated from the concentrations of alkalis measured in the solution after 5 min agitation at a w/c of 10; present as alkali sulphates.
[d] Present as solid solution in the major clinker phases, cf. Table 2.

Table 2
Alkalis, Mg and sulphate associated with the unhydrated clinker phases in the OPC calculated according to Table 1.3 in Taylor [10] and the phase composition (Table 1)

| | Na | K | Mg | $SO_3$ |
|---|---|---|---|---|
| | In mmol/100 g cement | | | |
| Alite | 0.48 | 0.8 | 27.1 | 1.06 |
| Belite | 0.17 | 2.9 | 3.2 | 0.38 |
| Aluminate | 0.52 | 1.3 | 4.9 | |
| Ferrite | 0.07 | 0.4 | 10.6 | |
| Total | 1.2 | 5.4 | 45.9 | 1.4 |

Hydroxide concentrations were determined with a combined pH-electrode in undiluted samples; the pH electrode had been calibrated against KOH solutions of known concentrations. The total concentrations of Al, Ba, Ca, Cr, Fe, K, Li, Mg, Mo, Na, Si, Sr, S and Zn were determined with ICP-OES in samples diluted at least by a factor 4 with diluted $HNO_3$ to prevent the precipitation of solids. The solid fraction was crushed and ground in acetone, dried at 40 °C and then used for XRD and thermogravimetric analysis (TGA). TGA was carried out in nitrogen on about 10 mg of powdered cement pastes at 3 °C/min up to 220 °C and at 10 °C/min up to 640 °C. The amount of pore solution present was calculated from the difference of the total weight loss during TGA between the samples washed with acetone and untreated samples; the amount of $Ca(OH)_2$ present from the weight loss between 500–580 °C in the TGA results and from the extracted amount of Ca determined according to the method of Franke [11].

## 3. Experimental results

### 3.1. XRD and TGA data

The extent of cement hydration was estimated based on the changes in the peak intensities of the crystalline phases in XRD patterns as well as on the changes observed by DTG/TGA. The DTG/TGA analysis of the unhydrated sample shows the presence of gypsum and hemihydrate. After 30 min reaction time hemihydrate is dissolved, gypsum is consumed within the first day. Increasing amounts of ettringite, C-S-H and portlandite could be observed in the hydrated samples. The presence of DTG peaks at 200, 260 and 430 °C are consistent with the presence of an AFm phase such as calcium monosulphoaluminate or calcium monocarboaluminate [10,12] after 7 days; the weak peaks at 260 and 430 °C could also be due (in part) to a hydrotalcite phase [10].

A semi-quantitative evaluation of the XRD patterns (Fig. 1) shows that the alite and aluminate phase hydrate relatively fast and have mostly disappeared by 300 days. The observed hydration rates for belite and ferrite phase hydration are significantly slower. The anhydrite and

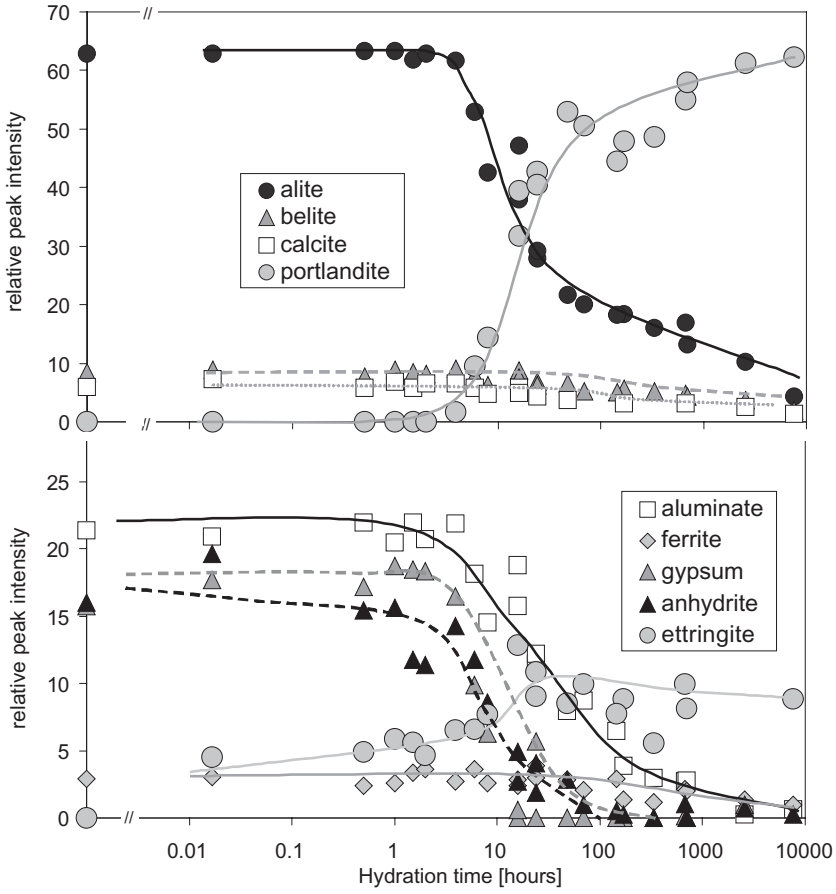


Fig. 1. Semi-quantitative evaluation of XRD patterns of the solid phase after different hydration times. Lines are intended as eye guides only. Samples have been washed with acetone and dried at 40 °C.

gypsum initially present dissolve slowly as the sulphate in solution is continuously removed by the precipitation of ettringite and/or calcium monosulphoaluminate; similarly, the amount of calcite decreases slowly with time, presumably forming calcium monocarboaluminate. Precipitating ettringite is detected after only a few minutes of hydration, portlandite after 4 h, and calcium monocarboaluminate after 100 days. Other phases could not be clearly identified in the XRD analysis as many of the peaks overlap; however, it is possible that poorly crystalline AFm and hydrotalcite phases are present within the hydrated cement. Isothermal calorimetry indicated the onset of the acceleration period at 2 h and a maximal heat evolution after 11 h.

### 3.2. Elemental concentrations in the pore solution of OPC

During the first 7 h the composition of pore solution is dominated by K, S, hydroxide, Na and Ca (Table 3). The high concentrations of K, Na and S observed after only a few minutes are due to the fast dissolution of alkali-sulphate phases. The observed slow increase of alkali concentrations is (i) due to the decrease of pore solution—as the water present is consumed by the different hydration products—and (ii) due to the slow release of alkalis trapped in the slowly-hydrating clinker minerals (cf. Table 2). The bulk of sodium and potassium ultimately ends up in the solution, except a portion which is adsorbed on C-S-H. In high potassium cements some potassium is also precipitated as syngenite ($K_2Ca(SO_4)_2{\cdot}H_2O$) at early ages, although it dissolves again later as the sulphate ions are consumed by reaction with the aluminate phases.

The concentrations of Ca, S and hydroxide remain more or less constant during the first 7 h as their concentrations are limited by the presence of anhydrite ($CaSO_4$) and portlandite ($Ca(OH)_2$). The concentrations of Al, Fe and Si (they constitute together more than 10 wt.% of the OPC) in the pore solution are always very low. The drops observed for Fe, Al and Si concentrations during the first hour are presumably related to the well-known precipitation of (relatively metastable) initial hydrates around the cement grains.

Larger changes in the composition of the pore solution of the OPC are observed after roughly 12 h: Ca and S concentrations decrease drastically, while the concentrations of hydroxide, Si, and Al all increase at the same time. This decrease in calcium and sulphur concentrations coincides roughly with the disappearance of anhydrite and gypsum from the XRD patterns. The observed trends in K, Na, Ca,

Table 3
Measured total concentrations in the pore solutions gained from OPC (w/c=0.5)

| Time [h] | K | Na | Li | Ca | Sr | Ba | Cr | Mo | Fe | Al | Si | S | $OH^-$ |
|---|---|---|---|---|---|---|---|---|---|---|---|---|---|
| | mM | | | | | | | | | | | | |
| 0.02 | 320 | 26 | 0.35 | 21.1 | 0.15 | 0.015 | 0.36 | 0.021 | 0.143 | 0.04 | 0.14 | 161 | 85 |
| 0.5 | 350 | 28 | 0.46 | 21.1 | 0.16 | 0.006 | 0.40 | 0.025 | 0.021 | 0.03 | 0.10 | 163 | 120 |
| 1 | 360 | 28 | 0.46 | 22.2 | 0.17 | 0.006 | 0.41 | 0.025 | 0.014 | 0.03 | 0.09 | 156 | 130 |
| 1.5 | 360 | 28 | 0.46 | 22.9 | 0.17 | 0.006 | 0.41 | 0.021 | 0.007 | 0.03 | 0.07 | 150 | 150 |
| 2 | 360 | 29 | 0.52 | 24.1 | 0.18 | 0.006 | 0.41 | 0.025 | 0.007 | 0.03 | 0.06 | 147 | 150 |
| 4 | 360 | 29 | 0.52 | 23.0 | 0.24 | 0.003 | 0.36 | 0.017 | 0.007 | 0.03 | 0.07 | 150 | 150 |
| 6 | 340 | 27 | 0.52 | 22.1 | 0.29 | 0.003 | 0.25 | 0.008 | <0.007 | 0.03 | 0.06 | 139 | 150 |
| 7 | 350 | 30 | 0.63 | 21.3 | 0.30 | 0.006 | 0.22 | 0.008 | <0.007 | 0.03 | 0.07 | 151 | 150 |
| 16 | 430 | 32 | 0.58 | 9.5 | 0.15 | <0.003 | 0.10 | <0.004 | <0.007 | <0.004 | 0.07 | 136 | 200 |
| 26 | 430 | 44 | 0.75 | 4.2 | 0.08 | <0.003 | 0.07 | <0.004 | <0.007 | <0.007 | 0.17 | 83 | 360 |
| 69 | 480 | 49 | 0.69 | 2.0 | 0.05 | <0.003 | 0.04 | <0.004 | <0.007 | <0.007 | 0.21 | 9 | 480 |
| 144 | 520 | 55 | 0.81 | 2.1 | 0.05 | <0.003 | 0.05 | <0.004 | <0.007 | 0.09 | 0.24 | 10 | 520 |
| 336 | 510 | 56 | 0.86 | 1.9 | 0.05 | <0.003 | 0.05 | <0.004 | <0.007 | 0.09 | 0.23 | 9 | 560 |
| 696 | 560 | 63 | 0.92 | 1.2 | 0.03 | <0.003 | 0.05 | <0.004 | <0.007 | 0.12 | 0.27 | 11 | 540 |
| 2520 | 650 | 57 | 0.86 | 1.5 | 0.05 | <0.003 | 0.06 | <0.004 | <0.018 | 0.04 | 0.21 | 17 | 570 |
| 7608 | 640 | 65 | 1.2 | 1.5 | 0.05 | n.a. | 0.06 | n.a. | <0.018 | 0.11 | 0.21 | 16 | 590 |
| Concentrations in filtered blank solutions | | | | | | | | | | | | | |
| | 0.06 | 0.05 | <0.006 | 0.03 | <0.005 | <0.003 | <0.004 | <0.004 | <0.007 | <0.01 | 0.01 | 0.04 | – |

The values for $OH^-$ refer to the free concentrations measured in the pore solutions.
The measured concentrations of Zn and Mg were in all samples below the respective detection limits of 0.001 and 0.02 mM, respectively. Total S is determined by ICP-OES independent of its redox state. In pure OPC system investigated, S is present in the oxidized form as sulphate.

S, Si, Al and hydroxide concentration are consistent with the observations reported by other authors [8,13–15]. The Ca, Si, Al, and hydroxide concentrations reported in the literature are comparable with each other and with our results, while K, Na and S concentrations differ depending on the composition of cement and the water/cement ratio used. However, the pore solution development follows in all cases roughly the same trends.

Thermodynamic calculations (see details below) indicate that during the first hours, the pore solution of this cement is in equilibrium with anhydrite, and thus oversaturated with respect to gypsum (Fig. 2). A relatively slow gypsum precipitation rate at low oversaturation ratios [16]—coupled with the calcium and sulphate consumption by the precipitation of ettringite—could explain the continued coexistence of gypsum and anhydrite, as observed in the XRD data, during the first hours of cement hydration. Similarly, the solutions are oversaturated with respect to portlandite (Fig. 2), ettringite and syngenite as the release of Ca and Al from the hydration of the clinker phases into the solution is faster than the precipitation of these solids from the modestly oversaturated solutions. Oversaturation of cementitious pore solutions with respect to portlandite, gypsum, ettringite and/or syngenite during the early cement hydration has been observed in several previous studies [4,8,13,17].

The concentrations of a number of other "trace" elements were also measured in the cement pore solutions (Table 3). Li shows a similar increase with time as observed for Na and K. The concentrations of Sr and Ba decrease after 1 day as observed also for Ca. Similarly, the

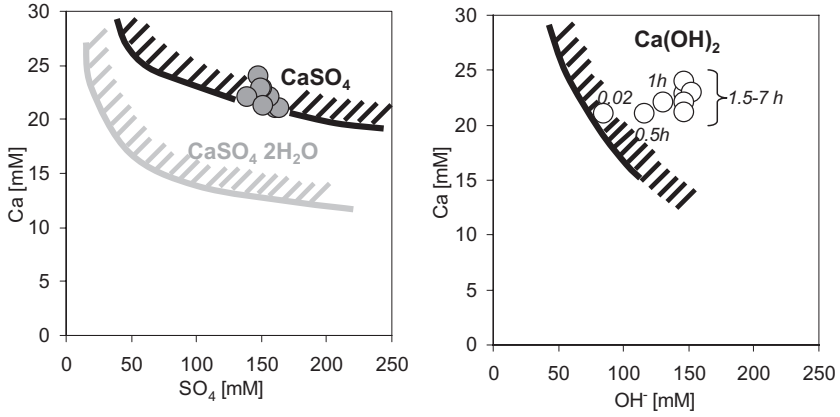


Fig. 2. Measured calcium, sulphate, and hydroxide concentrations in the pore solution during the first 7 h compared with the calculated solubility of gypsum ($CaSO_4 \cdot 2H_2O$), anhydrite ($CaSO_4$) and portlandite ($Ca(OH)_2$) in the pore solution of OPC.

concentrations of Mo and Cr, which under these alkaline conditions are only likely to be present in solution as $MoO_4^{2-}$ and $CrO_4^{2-}$, both decrease after 1 day. Both $MoO_4^{2-}$ and $CrO_4^{2-}$, are expected to show similar trends in their concentrations as S, as they can substitute for $SO_4^{2-}$ in AFt and AFm phases [18–20] due to their identical charge, similar structure and comparable ionic radii.

## 4. Modelling approach

When OPC is brought into contact with water, the soluble alkali sulphates dissolve readily releasing K, Na and S into the solution. Less soluble solids such as gypsum, anhydrite, and calcite dissolve partially until equilibrium with the pore solutions is reached. In addition, the slow hydration of the clinker phases releases continuously Ca, Si, Al, Fe and (hydr)oxide into the solution. Si and Ca react to precipitate as C-S-H phase, while Al and Fe react with the hydroxide, S, C and Ca present to yield AFt, AFm or other hydroxide phases. The dissolution rate of the clinker phases determines the amount of Ca, Al, Fe, Si and hydroxide released into the solution and thus the rate of the precipitation of AFt and AFm, C-A-H and C-S-H phases.

Thus, the model used is based

(i) On the measured composition of the OPC used in this work (cf. Tables 1 and 2),
(ii) On the calculated dissolution rates of the clinker phases as kinetic input, and
(iii) On using the Gibbs free energy minimisation program GEMS [21] together with the internally consistent thermodynamic data set of [22] expanded with additional data for solids that are expected to form under cementitious conditions (thermodynamic constants used are summarized in the Appendix).

### 4.1. Modelling the dissolution of the cement clinker phases

The hydration of cements can be assumed to take place via dissolution and precipitation processes. Different models exist to describe the hydration and/or dissolution rates of the phases in Portland cements. One can distinguish between models which include both dissolution and precipitation reactions, e.g. Refs. [23,24], and models which are based on the dissolution reactions only [25–28]. The latter authors derived (based on quantitative X-ray measurements) empirical expressions which estimate the degree of dissolution of each clinker mineral as a function of time; the differences between the results of these four different approaches are generally rather small. However, the mathematical expressions used by Refs. [25,27,28] imply that essentially no dissolution of any of the clinker phases occurs during the first few hours, while the approach of Parrot and Killoh [26] has no such restrictions and describes the rate $R$ of the hydration of the individual clinker phases by a set of equations, where the lowest value of $R$ at the time $t$ is considered as the rate controlling step:

nucleation and growth

$$R_t = \frac{K_1}{N_1}(1-\alpha_t)(-\ln(1-\alpha_t))^{(1-N_1)} \text{ or} \quad (1)$$

$$\text{diffusion } R_t = \frac{K_2 \times (1-\alpha_t)^{2/3}}{1-(1-\alpha_t)^{1/3}} \text{ or} \quad (2)$$

$$R_t = K_3 \times (1-\alpha_t)^{N_3} \quad (3)$$

The degree of hydration $\alpha$ at time $t$ (in days) is then expressed as $\alpha_t = \alpha_{t-1} + \Delta t \cdot R_{t-1}$. In this paper, the empirical expressions (Eqs. (1) (2) (3)) as given by Parrot and Killoh [26] are used together with their values of $K_1$, $N_1$, $K_2$, $K_3$ and $N_3$ as compiled in Table 4. The influence of w/c according to $f(w/c) = (1 + 4.444 * (w/c) - 3.333 * \alpha_t)^4$; for $\alpha_t > 1.333 * (w/c)$ [26] as well as the influence of the surface area on the initial hydration is included using the data given in Parrot and Killoh [26]. The set of equations describes the progress of dissolution in OPC well as can be seen by comparing the calculated progress of dissolution with the results of our semi-quantitative XRD results (Fig. 3).

### 4.2. Release and uptake of alkalis, sulphate and magnesium during hydration

In cement clinkers some substitution of Ca, Si, Al, and Fe by Na, K, Mg, Fe, Al, P or S is often observed [10]. These elements associated with clinker phases are released into the solution only upon the dissolution of the respective clinker phase. For the model calculations the distribution of K, Na, Mg and S between the clinker phases is taken into account as described in Taylor [10] (cf. Table 2).

The alkalis released from the dissolution of the alkali sulphates and during the slow dissolution of the clinkers, partition between the solution and the precipitating C-S-H phases. The quantification of the amount of alkalis taken up by the C-S-H phases has been discussed by different authors [3,4,7,28–30]. While Sinitsyn et al. [7] modelled the Na uptake by C-S-H by the introduction of a Na-Ca-hydrate end

Table 4
Parameters from Parrot and Killoh [26] used to calculate the hydration of the individual clinker phases as a function of time

| Parameter[a] | Clinkers | | | |
|---|---|---|---|---|
| | Alite | Belite | Aluminate | Ferrite |
| $K_1$ | 1.5 | 0.5 | 1.0 | 0.37 |
| $N_1$ | 0.7 | 1.0 | 0.85 | 0.7 |
| $K_2$ | 0.05 | 0.006 | 0.04 | 0.015 |
| $K_3$ | 1.1 | 0.2 | 1.0 | 0.4 |
| $N_3$ | 3.3 | 5.0 | 3.2 | 3.7 |

[a] All parameters from Ref. [26] for OPC.

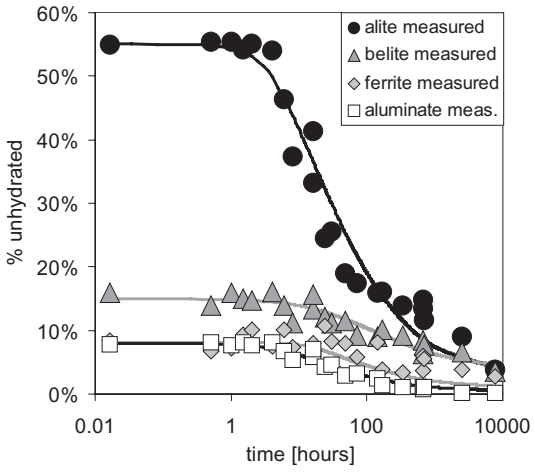


Fig. 3. Comparison of the calculated amount of clinker present in OPC as a function of hydration time with the results of the semi-quantitative evaluation of the XRD patterns. Calculations are based on Eqs. (1) (2) (3) and the data given in Table 4. Experimental data are scaled such that the percentages in the unhydrated cement correspond to the calculated composition of the cement as given in Table 1.

member ($CaNaH_2SiO_4OH$) into the C-S-H solid solution series, others [28,30] used empirical partition coefficients. Sinitsyn et al. [7] as well as Reardon [4] concluded that the uptake of alkalis in cementitious systems is significantly weaker than in pure C-S-H phases. In contrast, Brouwers and van Eijk [31] found no difference in the uptake of alkalis by C-S-H phases and OPC by comparing model calculations based on the data of Refs. [28] and [30] with experimental pore solutions gained from OPC. Hong and Glasser [29,30] determined experimentally the Na and K partitioning in C-S-H and C-A-S-H gels and derived distribution ratios $R_d$ from these data. The distribution ratios $R_d$ describe the partitioning of alkalis between C-S-H and solution as a function of the alkali concentration in the solution according to:

$$R_d = \frac{c_s w}{c_d s}\left[\frac{\text{ml}}{\text{g}}\right] \quad (4)$$

where $c_s$ corresponds to the alkali concentration in the solid phase [mol/l], $c_d$ to the alkali concentration in the solution [mol/l] and w/s is the water/solid ratio in ml/g.

Hong and Glasser [30] observed in their experiments with C-S-H (i) that steady state distribution is attained rapidly, (ii) that for both Na and K the same $R_d$ value is obtained and (iii) that the value of $R_d$ does not depend on the alkali concentration but only on the C/S ratio.[2] The distribution ratio $R_d$ decreases with increasing C/S ratio (from 4.5 ml/g at C/S=0.85 to 0.42 ml/g at C/S=1.8).

[2] Hong and Glasser [30] reported at very high K and Na concentrations (>300 mM) a decrease of the uptake due to saturation effects. However, as we use a significantly higher solid/water ratio such a decrease due to saturation effects will occur only at even higher alkali concentrations.

The uptake of alkalis by the precipitating C-S-H phases in fresh cements—which exhibit a high C/S ratio— is calculated in this paper using a distribution ratio $R_d$ of 0.42 ml/g C-S-H gel for both Na and K corresponding to the mean of the values determined by Ref. [30] at a C/S ratio of 1.8.

## 5. Modelling results

### 5.1. Thermodynamic equilibrium

Using the calculated composition of the cement (Tables 1 and 2) and the dissolution of the clinkers as a function of time (cf. Table 4) as input parameters, the evolution of the pore solution and the precipitating solids as a function of time were calculated assuming thermodynamic equilibrium between the liquid phase and precipitating solids. The calculations were carried out using the Gibbs energy minimisation program GEMS [21]; the amount of free pore water was calculated from the original water content of the cement/water system, the progress of the dissolution (hydration) and the composition of the precipitated solids.

The calculated changes in the pore solution during cement hydration agree with the observations in the pore solution of the OPC used (Fig. 4). At the employed w/c of 0.5, the alkali sulphates present dissolve completely in the pore solution, while anhydrite and calcite dissolve partly until equilibrium with the pore solution is reached. Sulphate is removed from the solution as it precipitates as ettringite; its concentration in solution, however, remains constant as long as anhydrite and/or gypsum are present. The thermodynamic model predicts, based on the rate of aluminate hydration calculated from Ref. [26], a decrease of S and Ca-concentration only after roughly 12 h as the calcium sulphate phases are depleted (cf. Figs. 4-6).

The analysis of the pore solution has shown that the solutions are oversaturated with respect to gypsum, portlandite and ettringite during the first 12 h but are in equilibrium with the dissolution of anhydrite (cf. Fig. 2), as the precipitation from the only slightly oversaturated solutions seems to proceed in the investigated system relatively slow. Thus, as indicated in Fig. 4, the presence of anhydrite ($CaSO_4$) but not of gypsum ($CaSO_4{\cdot}2H_2O$) is considered in the calculations. Similarly, the solutions are initially oversaturated with respect to syngenite, portlandite and ettringite, resulting in the calculated hydroxide, Ca and Al concentrations being somewhat lower then the measured values (Fig. 4).

Such an oversaturation with respect to portlandite, gypsum, syngenite or ettringite during early cement hydration has also been observed in other studies [4,8,17]. A more precise prediction of concentrations in the pore solution during early cement hydration would be obtained by the use of a kinetic model for the precipitation, where the rates of nucleation and precip-

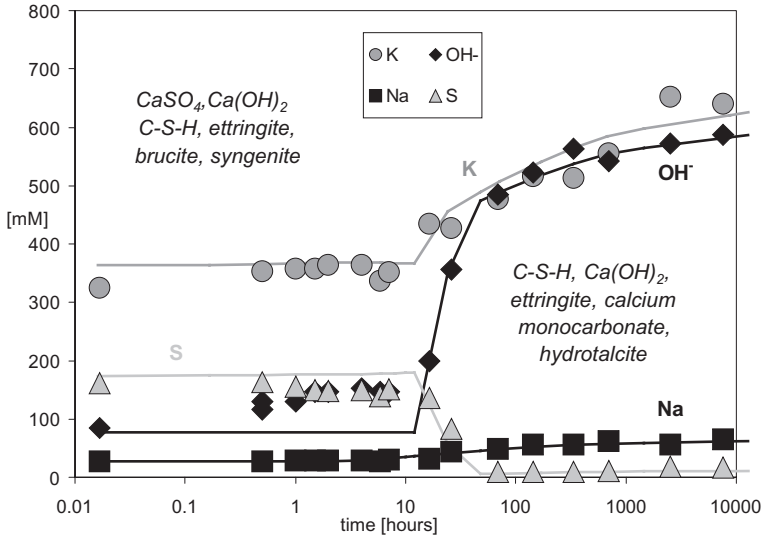


Fig. 4. Comparison of the modelled evolution of the pore solution during the hydration of OPC assuming thermodynamic equilibrium with the concentrations measured in the pore solution of OPC. The solid phases in equilibrium with the calculated pore solution are indicated in italics. Note that free concentrations are only given for hydroxide, while all other concentrations refer to total dissolved elemental concentrations.

itation could be calculated as a function of the relative oversaturation in the solution for each of the solids. Due to the lack of kinetic data for many of the solids, a more simple approach has been used here, as discussed in the next section, assuming during the first 12 h of the cement hydration the precipitation of somewhat "less crystalline" (more soluble) solids than the pure standard phases, which is equivalent to the assumption of a constant degree of oversaturation.

### 5.2. Oversaturation during the first 12 h

Based on the comparison of experimental and modelled results for Ca and hydroxide, a constant (over)saturation ratio $=(IAP/K_{S0})^{1/n}$ of $10^{0.15}$ was applied to all calculations referring to the first 12 h, increasing the solubility product of all precipitating solids (i.e. portlandite, gypsum, syngenite, brucite, tobermorite-II, jennite, ettringite and Fe-ettringite) by $n$ times 0.15 log units, where $n$ corresponds to the number of ions in the formula unit of the respective mineral and IAP to the ion activity product (for reactions and the equilibrium constants cf. Table A.1). Thus, assuming the precipitation of less crystalline and more soluble solids during the first 12 h, a better agreement between the calculated Ca, hydroxide and S concentrations in the pore solution and the measured data is obtained (Fig. 5) and no gypsum is predicted to precipitate under these conditions. Only the calculated Al and Fe concentrations are still lower than the measured concentrations during the first 12 h, indicating an even stronger oversaturation with respect to ettringite than considered in the calculations. A similar large oversaturation relative to ettringite has also been observed by Rothstein et al. [8] during the first 6 h of their experiments.

The modelled composition of the pore solution (Fig. 5) is constant during the first 12 h and dominated by the presence of K, S, and hydroxide, as observed in the experimental data. Also the calculated concentrations Na, Ca and Si concentrations agree well with the measured concentrations (Fig. 5). The model calculations predict the presence of anhydrite and calcite as well as the precipitation of portlandite, C-S-H, ettringite and small amounts of brucite during the first few hours (Fig. 6) which agrees well with observations made in the TGA and XRD analysis (cf. Fig. 1). Only brucite has not been detected, which might be due to the low fraction of brucite likely to be present (<1%) or due to the uptake of Mg by the newly forming C-S-H phase (which is not considered in the model).

### 5.3. Solid and liquid phase after 1 day

The prediction of K and Na concentrations as a function of time reproduces the measured data very well (Fig. 5). The concept of alkali release, pore solution decrease and uptake of alkalis by using the distributions ratio determined by Hong and Glasser [30] for C-S-H describes the measured K and Na concentrations in the presence of OPC very well. This suggests that C-S-H is in fact the main binder of alkalis in hydrating OPC as already suggested by Brouwers and van Eijk [31] based on data of another OPC. The concentration of hydroxide after 1 day or longer is dominated by the concentrations of K and Na present and the agreement between measured and predicted values is excellent.

The thermodynamic modelling in combination with the calculated hydration rates [26] predicts the depletion of anhydrite and gypsum after half a day and a drastic decrease of the sulphate concentrations in the pore solutions as

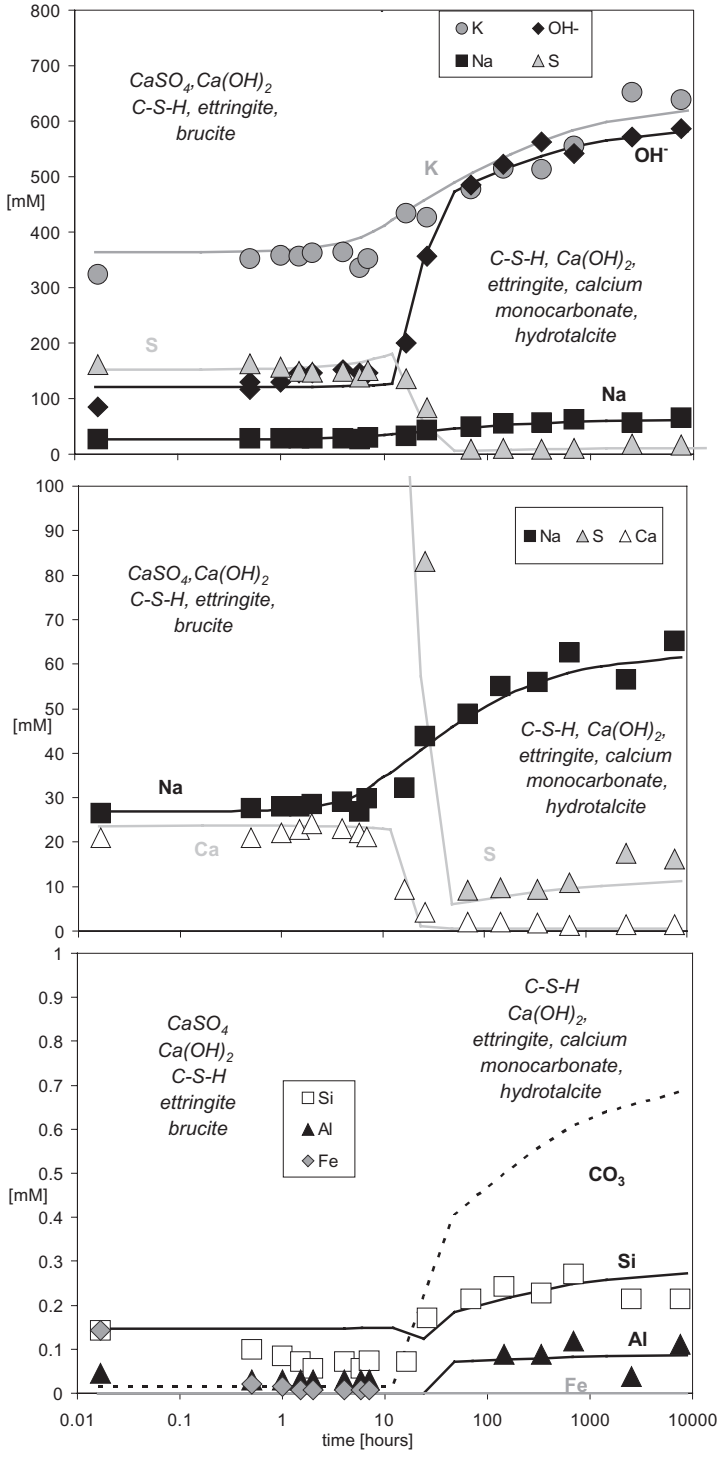


Fig. 5. Comparison of the modelled evolution of the pore solution during the hydration of OPC assuming during the first 12 h the precipitation of less stable solids (see text) with the concentrations measured in the pore solution of OPC. To ease readability the data are plotted using different concentrations scales. Measured Fe concentrations after 24 h or longer are below the detection limit and thus not indicated in the graph. The solid phases in equilibrium with the calculated pore solution are indicated in italics.

ettringite continues to precipitate until sulphate in the solution is depleted (Figs. 5 and 6). At the same time, as the electroneutrality of the solution is maintained, hydroxide concentration and thus the pH value increases drastically. This leads to a decrease in Ca concentration due to the common ion effect (portlandite equilibrium) while the calculated Al, Si and also Fe concentrations increase. The calculated Si, Ca, S and Al concentrations after 1 day or longer agree well with the experimental findings (Fig. 5) while the calculated concentrations of Fe and Mg with 0.2

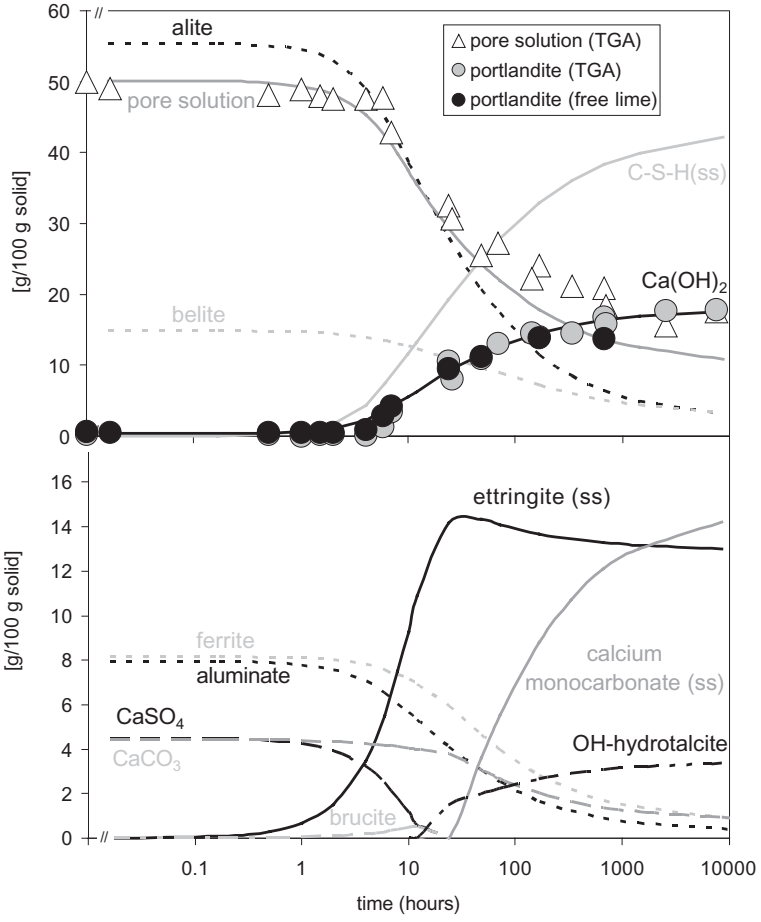


Fig. 6. Modelled evolution of the solid phases during the hydration of OPC (w/c=0.5) assuming thermodynamic equilibrium with the aqueous phase as given in Fig. 5 compared with the experimentally determined amount of pore solution and portlandite. In order to ease the comparison with XRD and TGA data, the values refer to 100 g of solid; i.e. the mass of the solid phase increases with time as more and more hydration product precipitates and the amount of pore solution is reduced (ss=solid solution).

μM and 1 nM, respectively, are well below the respective detection limits of these elements in the experimental pore solutions (Table 3).

The calculations also predict carbonate concentrations of up to 0.7 mM in the pore solution. Carbonate originates principally from calcite in the cement. In the calculations, no atmospheric $CO_2$ was assumed to enter into the system. As the pore solutions were not analysed for carbonate, the calculations cannot be verified against experimental data.

The changes in the composition of pore solution after half a day lead also to changes in the modelled phase assemblage; calcium monocarbonate[3] and hydrotalcite are predicted to precipitate while at the same time calcite is consumed (Fig. 6). With time, more and more C-S-H and portlandite are predicted to form while the precipitation of ettringite stops after roughly one day once all of the soluble sulphate (with exception of the very small portion still associated with the unhydrated clinker phases) is consumed.[4] These model predictions agree well with the TGA and XRD data of the experimental investigations (Fig. 1), where the amount of ettringite slightly decreases after 1 day, while the formation of C-S-H, portlandite, and AFm phase in the cement continues.

The slow dissolution of calcite as observed in the XRD data (Fig. 1) indicates that the observed AFm phase could in fact be calcium monocarbonate, even though calcium monocarboaluminate could be identified only after 100 days in the XRD data. The thermodynamic calculations show that calcium monocarbonate should form in preference to calcium monosulphoaluminate or other AFm phases in cementitious systems containing carbonates. This is in agreement with the experimental findings of Kuzel [32],

[3] The expression calcium monocarbonate is used in this paper for the solid solution between calcium monocarboaluminate and its Fe-containing analogue: $C_4(A,F)\bar{C}H_{11}$, see Appendix.

[4] Note that the quantities given in Fig. 6—in order to ease the comparison with the experimental evidence from the XRD and TGA data—refer to weight relative to 100 g of solid phase (including also the newly formed hydration products) and not to unhydrated cement paste; i.e. the absolute amount of ettringite remains more or less constant after 24 h, the relative amount, however, (as shown in Fig. 6) is decreasing as the weight of the solid fraction in the cement increases due to the precipitation of the hydration products.

who showed that in the presence of sufficient carbonate, calcium mono-or hemicarboaluminate formation prevents the formation of calcium monosulphoaluminate from ettringite. However, even though thermodynamic modelling predicts only the precipitation of calcium monocarbonate, it cannot be excluded that other AFm phases may also precipitate as the thermodynamic models which describe the solid solution behaviour of the different AFm phases are only a rough approximation (for a more detailed discussion of the interaction of the AFm phases, see Appendix) and the experimental evidence is very limited. The model calculates significant solid solutions (Al, Fe) for precipitated ettringite and calcium monocarbonate.

It is interesting to note, that the thermodynamic calculations also indicate, that in the presence of calcite, calcium monocarboaluminate is more stable than the hydrogarnet phases and thus no hydrogarnet is expected to form. In the absence of calcite (and other carbonate sources), thermodynamically stable hydrogarnet phases should precipitate. If we neglect the formation of hydrogarnet phases for kinetic reasons, an AFm solid solutions of $C_4(A,F)\bar{S}H_{12}$, $C_4(A,F)H_{13}$, $C_2(A,F)H_8$ and mainly $C_2(A,F)SH_8$ is predicted to precipitate in the cement water system (Fig. 7). However, thermodynamic modelling also shows that upon carbonation, these AFm phases will be replaced by calcium monocarbonate as has been observed by Kuzel [32] in experiments with carbonate-free Portland cements.

MgO present in cementitious systems is predicted to precipitate initially as brucite ($Mg(OH)_2$) and later to convert to hydrotalcite (Fig. 6), once the soluble sulphates have been exhausted. Whether brucite and hydrotalcite are actually formed or whether most of the Mg is incorporated into the C-S-H phase is difficult to predict. Taylor [10], however, concluded, based on TEM and X-Ray evidence, that Mg is generally associated with Al and Fe to form hydrotalcite-like phases.

The good agreement between calculations and experimental results indicates that the most important processes and phases have been included in the model system even though some of their thermodynamic data had to be estimated or are completely missing. In particular, we lack data for the Fe-containing AFm and AFt-phases as well as for the hydrotalcite and hydrogarnets. In addition, we lack data for a thermodynamic description of the uptake of ions such as Na, K, Al, Fe, Mg and sulphate in C-S-H, which may limit the applicability of the model particularly for systems where a more significant uptake of different ions in the C-S-H structure is observed (e.g. in slag systems).

## 6. Conclusions and outlook

A thermodynamic model is developed and applied to calculate the composition of the pore solution and the development of the solid phase during hydration. A simple kinetic model for the rates of consumption of the individual clinker phases is used as time dependent input.

The modelled data compare well with the measured compositions of the pore solutions obtained from OPC as well as with TGA and XRD data on the solid phases. The good agreement between calculations and experimental results indicates that chemical equilibrium calculations can adequately predict the hydrates formed in cement systems and that all of the important phases were included in our model even though some thermodynamic data had to be estimated or are still missing. The results serve as an important reminder of the fact that calcium monocarboaluminate is thermodynamically more stable than hydrogarnet or other AFm phases under typical cement conditions. Only in the absence of carbonate, are either hydrogarnets or other AFm phases predicted to precipitate or is ettringite expected to disappear.

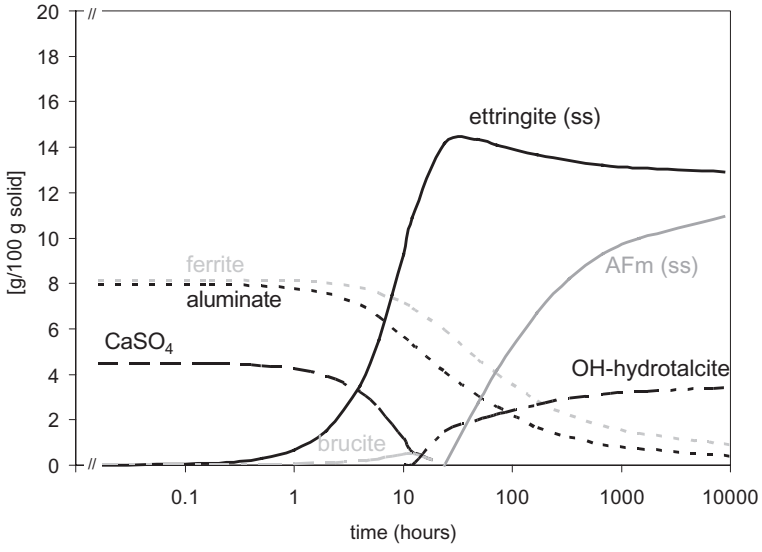


Fig. 7. Modelled evolution of the solid phases during the hydration of OPC (w/c=0.5) assuming the absence of carbonate (ss=solid solution).

Our thermodynamic model could also be used for predicting the influence of changes in the original cement composition (such as the presence or absence of calcite) and the environment on the hydrate assemblage and thus the properties of the resulting hardened cement pastes. Thermodynamic modelling can provide a deeper understanding of the interactions between the different components and help with further optimisation of complex, multicomponent cementing systems.

## Acknowledgements

The active support of Luigi Brunetti from the section concrete/construction chemistry, EMPA, during the laboratory work, the careful analysis of R. Figi, P. Lienemann and their co-workers from the section inorganic chemistry/characterisation of solids, EMPA, are gratefully acknowledged.

## Appendix A. Thermodynamic data

All calculations are carried out using the GEMS Gibbs energy minimisation code [21]. The default database of the GEMS code is based on the recent PSI chemical thermodynamic database [22] (which is reproduced in Table A.1) supplemented with "complementary" data from the SUPCRT database [33–36]. Activity coefficients of aqueous species $\gamma_j$ are computed with the built-in expanded

Table A.1
Chemical equilibrium constants used for modelling the composition of the pore solutions

| | log $K$ or log $\beta$ | Reference |
|---|---|---|
| *Aqueous species* | | |
| $Ca^{2+}+H_2O \Leftrightarrow CaOH^{+}+H^{+}$ | −12.78 | [22] |
| $Ca^{2+}+SO_4^{2-} \Leftrightarrow CaSO_4^{0}$ | 2.44 | [59] |
| $Ca^{2+}+HCO_3^{-} \Leftrightarrow CaHCO_3^{+}$ | 1.106 | [22] |
| $Ca^{2+}+HCO_3^{-} \Leftrightarrow CaCO_3^{0}+H^{+}$ | −7.105 | [22] |
| $Ca^{2+}+H_2SiO_4^{2-} \Leftrightarrow CaH_2SiO_4^{0}$ | 4.60 | [22] |
| $Ca^{2+}+H_3SiO_4^{-} \Leftrightarrow CaH_3SiO_4^{+}$ | 1.20 | [22] |
| $Mg^{2+}+H_2O \Leftrightarrow MgOH^{+}+H^{+}$ | −11.44 | [22] |
| $Mg^{2+}+SO_4^{2-} \Leftrightarrow MgSO_4^{0}$ | 2.37 | [22] |
| $Mg^{2+}+HCO_3^{-} \Leftrightarrow MgHCO_3^{+}$ | 1.068 | [22] |
| $Mg^{2+}+HCO_3^{-} \Leftrightarrow MgCO_3^{0}+H^{+}$ | −7.349 | [22] |
| $Mg^{2+}+H_2SiO_4^{2-} \Leftrightarrow MgH_2SiO_4^{0}$ | 5.70 | [22] |
| $Mg^{2+}+H_3SiO_4^{-} \Leftrightarrow MgH_3SiO_4^{+}$ | 1.50 | [22] |
| $Na^{+}+H_2O \Leftrightarrow NaOH^{0}+H^{+}$ | −14.18 | [22] |
| $Na^{+}+SO_4^{2-} \Leftrightarrow NaSO_4^{-}$ | 0.70 | [22] |
| $Na^{+}+HCO_3^{-} \Leftrightarrow NaHCO_3^{0}$ | −0.25 | [22] |
| $Na^{+}+HCO_3^{-} \Leftrightarrow NaCO_3^{-}+H^{+}$ | −9.059 | [22] |
| $K^{+}+H_2O \Leftrightarrow KOH^{0}+H^{+}$ | −14.46 | [22] |
| $K^{+}+SO_4^{2-} \Leftrightarrow KSO_4^{-}$ | 0.85 | [22] |
| $H_2O \Leftrightarrow OH^{-}+H^{+}$ | −14.000 | [22] |
| $HCO_3^{-} \Leftrightarrow CO_3^{2-}+H^{+}$ | −10.329 | [22] |
| $HCO_3^{-}+H^{+} \Leftrightarrow H_2CO_3^{0}$ | 6.352 | [22] |
| $HCO_3^{-}+H^{+} \Leftrightarrow CO_2(g)+H_2O$ | 7.82 | [22] |
| $Al^{3+}+H_2O \Leftrightarrow Al(OH)^{2+}+H^{+}$ | −4.957 | [22] |
| $Al^{3+}+2H_2O \Leftrightarrow Al(OH)_2^{+}+2H^{+}$ | −10.594 | [22] |
| $Al^{3+}+3H_2O \Leftrightarrow Al(OH)_3^{0}+3H^{+}$ | −16.432 | [22] |
| $Al^{3+}+4H_2O \Leftrightarrow Al(OH)_4^{-}+4H^{+}$ | −22.879 | [22] |
| $Al^{3+}+H_3SiO_4^{-} \Leftrightarrow AlSiO(OH)_3^{2+}$ | 7.40 | [22] |
| $Al(OH)_4^{-}+H_4SiO_4^{0} \Leftrightarrow AlSiO(OH)_6^{-}+H_2O$ | 3.60 | [22] |
| $Al^{3+}+SO_4^{2-} \Leftrightarrow AlSO_4^{+}$ | 3.90 | [22] |
| $Al^{3+}+2SO_4^{2-} \Leftrightarrow Al(SO_4)_2^{-}$ | 5.90 | [22] |
| $Fe^{3+}+H_2O \Leftrightarrow Fe(OH)^{2+}+H^{+}$ | −2.19 | [22] |
| $2Fe^{3+}+2H_2O \Leftrightarrow Fe_2(OH)_2^{4+}+2H^{+}$ | −2.95 | [22] |
| $3Fe^{3+}+4H_2O \Leftrightarrow Fe_3(OH)_4^{5+}+4H^{+}$ | −6.30 | [22] |
| $Fe^{3+}+2H_2O \Leftrightarrow Fe(OH)_2^{+}+2H^{+}$ | −5.67 | [22] |
| $Fe^{3+}+3H_2O \Leftrightarrow Fe(OH)_3^{0}+3H^{+}$ | −12.56 | [22] |
| $Fe^{3+}+4H_2O \Leftrightarrow Fe(OH)_4^{-}+4H^{+}$ | −21.60 | [22] |
| $Fe^{3+}+H_3SiO_4^{-} \Leftrightarrow FeH_3SiO_4^{2+}$ | 9.70 | [22] |
| $Fe^{3+}+H^{+}+SO_4^{2-} \Leftrightarrow FeHSO_4^{2+}$ | 4.47 | [22] |
| $Fe^{3+}+SO_4^{2-} \Leftrightarrow FeSO_4^{+}$ | 4.04 | [22] |
| $Fe^{3+}+2SO_4^{2-} \Leftrightarrow Fe(SO_4)_2^{-}$ | 5.38 | [22] |
| $SiO_2(OH)_2^{2-}+H^{+} \Leftrightarrow SiO(OH)_3^{-}$ | 13.33 | [22] |
| $SiO_2(OH)_2^{2-}+2H^{+} \Leftrightarrow Si(OH)_4^{0}$ | 23.14 | [22] |

(continued on next page)

Table A.1 (*continued*)

| Minerals[1] | $G_f^\circ$ [kJ/mol][2] | Reactions | log $K_{S0}$ | Reference |
|---|---|---|---|---|
| *Carbonate or sulphate minerals* | | | | |
| Calcite | −1129.176 | $CaCO_3(s)+H^+ \Leftrightarrow Ca^{2+}HCO_3^-$ | 1.849 | [21,22] |
| Magnesite | −1029.275 | $MgCO_3(s)+H^+ \Leftrightarrow Mg^{2+}HCO_3^-$ | 2.041 | [21,22] |
| Anhydrite | −1322.42[2] | $CaSO_4(s) \Leftrightarrow Ca^{2+}+SO_4^{2-}$ | −4.41 | [59] |
| Gypsum | −1797.89[2] | $CaSO_4 2H_2O(s) \Leftrightarrow Ca^{2+}+SO_4^{2-}+2H_2O$ | −4.60* | [59] |
| Syngenite | −2884.91 | $K_2Ca(SO_4)_2H_2O(s) \Leftrightarrow Ca^{2+}+2K^++2SO_4^{2-}+H_2O$ | −7.2* | Calculated[3] |
| *C-S-H solid solutions and portlandite* | | | | |
| Silica, amorphous[4] | −848.903 | $SiO_2(am)+2H_2O \Leftrightarrow Si(OH)_4$ | −2.713 | [21,22] |
| Tobermorite-I[4] | −4370.50 | $Ca(OH)_2)_2(SiO_2)_{2.4}\cdot(H_2O)_2$(tob-I)$+0.4H_2O \Leftrightarrow 2Ca^{2+}+2.4SiO(OH)_3^-+1.6OH^-$ | −18.2 | Calculated[3] |
| Tobermorite-II[5] | −3277.87 | $Ca(OH)_2)_{1.5}(SiO_2)_{1.8}\cdot(H_2O)_{1.5}$(tob-II)$+0.3H_2O \Leftrightarrow 1.5Ca^{2+}+1.8SiO(OH)_3^-+1.2OH^-$ | −13.65* | Calculated[3] |
| Jennite[5] | −2353.70 | $Ca(OH)_2)_{1.5}(SiO_2)_{0.9}\cdot(H_2O)_{0.9}$(jen) $\Leftrightarrow 1.5Ca^{2+}+0.9SiO(OH)_3^-+2.1OH^-$ | −11.85* | Calculated[3] |
| Portlandite | −897.013 | $Ca(OH)_2(s)+2H^+ \Leftrightarrow Ca^{2+}+2H_2O$ | 22.80* | [21,22] |
| *AFt-phases* | | | | |
| Ettringite[6] | −15207.02 | $Ca_6Al_2(SO_4)_3(OH)_{12}\cdot 26H_2O(s) \Leftrightarrow 6Ca^{2+}+2Al(OH)_4^-+3SO_4^{2-}+4OH^-+26H_2O$ | −45.09* | Calculated[3] |
| Fe-ettringite[6] | −14313.22 | $Ca_6Fe_2(SO_4)_3(OH)_{12}\cdot 26H_2O(s) \Leftrightarrow 6Ca^{2+}+2Fe(OH)_4^-+3SO_4^{2-}+4OH^-+26H_2O$ | −49.41* | Estimated[7] |
| Tricarboaluminate[6] | −14535.96 | $Ca_6Al_2(CO_3)_3(OH)_{12}\cdot 26H_2O(s) \Leftrightarrow 6Ca^{2+}+2Al(OH)_4^-+3CO_3^{2-}+4OH^-+26H_2O$ | −41.3 | Calculated[3] |
| *AFm-phases* | | | | |
| $C_4AH_{13}$[8] | −7327.46 | $4CaO\cdot Al_2O_3\cdot 13H_2O(s) \Leftrightarrow 4Ca^{2+}+2Al(OH)_4^-+6OH^-+6H_2O$ | −25.56 | [49] |
| $C_4FH_{13}$[8] | −6433.66 | $4CaO\cdot Fe_2O_3\cdot 13H_2O(s) \Leftrightarrow 4Ca^{2+}+2Fe(OH)_4^-+6OH^-+6H_2O$ | −29.88 | Estimated[7] |
| $C_2AH_8$[8] | −4812.75 | $2CaO\cdot Al_2O_3\cdot 8H_2O(s) \Leftrightarrow 2Ca^{2+}+2Al(OH)_4^-+2OH^-+3H_2O$ | −13.56 | [49] |
| $C_2FH_8$[8] | −3918.95 | $2CaO\cdot Fe_2O_3\cdot 8H_2O(s) \Leftrightarrow 2Ca^{2+}+2Fe(OH)_4^-+2OH^-+3H_2O$ | −17.88 | Estimated[7] |
| $C_2ASH_8$[8] | −5709.63 | $2CaO\cdot Al_2O_3\cdot SiO_2\cdot 8H_2O(s) \Leftrightarrow 2Ca^{2+}+2Al(OH)_4^-+Si(OH)_3^-+OH^-+2H_2O$ | −20.49 | Calculated[3] |
| $C_2FSH_8$[8] | −4815.83 | $2CaO\cdot Fe_2O_3\cdot SiO_2\cdot 8H_2O(s) \Leftrightarrow 2Ca^{2+}+2Fe(OH)_4^-+Si(OH)_3^-+OH^-+2H_2O$ | −24.80 | Estimated[7] |
| $C_4A\bar{S}H_{12}$[8] | −7769.60 | $3CaO\cdot Al_2O_3\cdot(CaSO_4)\cdot 12H_2O(s) \Leftrightarrow 4Ca^{2+}+2Al(OH)_4^-+SO_4^{2-}+4OH^-+6H_2O$ | −27.70 | Calculated[3] |
| $C_4F\bar{S}H_{12}$[8] | −6875.80 | $3CaO\cdot Fe_2O_3\cdot(CaSO_4)\cdot 12H_2O(s) \Leftrightarrow 4Ca^{2+}+2Fe(OH)_4^-+SO_4^{2-}+4OH^-+6H_2O$ | −32.02 | Estimated[7] |
| $C_4A\bar{C}H_{11}$[9] | −7337.46 | $3CaO\cdot Al_2O_3\cdot(CaCO_3)\cdot 11H_2O(s) \Leftrightarrow 4Ca^{2+}+2Al(OH)_4^-+CO_3^{2-}+4OH^-+5H_2O$ | −31.47 | Calculated[3] |
| $C_4F\bar{C}H_{11}$[9] | −6443.66 | $3CaO\cdot Fe_2O_3\cdot(CaCO_3)\cdot 11H_2O(s) \Leftrightarrow 4Ca^{2+}+2Fe(OH)_4^-+CO_3^{2-}+4OH^-+5H_2O$ | −35.79 | Estimated[7] |
| $C_4A\bar{C}_{0.5}H_{12}$[10] | −7339.51 | $3CaO\cdot Al_2O_3(Ca(OH)_2)_{0.5}\cdot(CaCO_3)_{0.5}11.5H_2O(s) \Leftrightarrow 4Ca^{2+}+2Al(OH)_4^-+0.5CO_3^{2-}+5OH^-+5.5H_2O$ | −29.75 | Calculated[3] |
| $C_4F\bar{C}_{0.5}H_{12}$[10] | −6445.72 | $3CaO\cdot Fe_2O_3(Ca(OH)_2)_{0.5}(CaCO_3)_{0.5}11.5H_2O(s) \Leftrightarrow 4Ca^{2+}+2Fe(OH)_4^-+0.5CO_3^{2-}+5OH^-+5.5H_2O$ | −34.07 | Estimated[7] |
| *Hydrogarnets* | | | | |
| $C_3AH_6$[11] | −5019.34 | $3CaO\cdot Al_2O_3\cdot 6H_2O(s) \Leftrightarrow 3Ca^{2+}+2Al(OH)_4^-+4OH^-$ | −22.46 | [49] |
| $C_3FH_6$[11] | −4125.53 | $3CaO\cdot Fe_2O_3\cdot 6H_2O(s) \Leftrightarrow 3Ca^{2+}2Fe(OH)_4^-+4OH^-$ | −26.78 | Estimated[7] |
| *$CAH_{10}$* | | | | |
| $CAH_{10}$ | −4622.33[2] | $CaO\cdot Al_2O_3\cdot 10H_2O(s) \Leftrightarrow Ca^{2+}+2Al(OH)_4^-+6H_2O$ | −7.49 | [53] |
| *Aluminum and iron hydroxides* | | | | |
| $Al(OH)_3$(am.) | −1143.21[2] | $Al(OH)_3(am)+OH^- \Leftrightarrow Al(OH)_4^-$ | 0.24 | [53] |
| Gibbsite | −1150.986 | $Al(OH)_3(s)+3H^+ \Leftrightarrow Al^{3+}+3H_2O$ | 7.76 | [21,22] |
| $Fe(OH)_3$(am.) | −700.194 | $Fe(OH)_3(am)+3H^+ \Leftrightarrow Fe^{3+}+3H_2O$ | 5.00 | [21,22] |
| $Fe(OH)_3$(microcr) | −711.610 | $Fe(OH)_3(mic)+3H^+ \Leftrightarrow Fe^{3+}+3H_2O$ | 3.00 | [21,22] |

Table A.1 (*continued*)

| Minerals[1] | $G_f^\circ$ [kJ/mol][2] | Reactions | log $K_{S0}$ | Reference |
|---|---|---|---|---|
| *Magnesium-phases* | | | | |
| Brucite | −832.227 | $Mg(OH)_2(s)+2H^+ \Leftrightarrow Mg^{2+}+2H_2O$ | 16.84* | [21,22] |
| OH-hydrotalcite (cr) | −6394.56 | $Mg_4Al_2(OH)_{14}\cdot 3H_2O(cr) \Leftrightarrow 4Mg^{2+}+2Al(OH)_4^-+6OH^-+3H_2O$ | −56.02 | Calculated[3] |
| $CO_3$-hydrotalcite | −6342.97 | $Mg_4Al_2(OH)_{12}\cdot CO_3\cdot 2H_2O(s) \Leftrightarrow 4Mg^{2+}+2Al(OH)_4^-+CO_3^{2-}+4OH^-+2H_2O$ | −51.14 | [58] |

Reactions constants for aqueous species as compiled in [22].
[1]Cement chemistry short-hand notations were used, where applicable C=CaO; M=MgO; S=$SiO_2$; A=$Al_2O_3$; F=$Fe_2O_3$; H=$H_2O$; $\bar{S}$=$SO_3$; $\bar{C}$=$CO_2$; [2]$G_f^\circ$ values calculated from log $K_{S0}$ values; [3]See text and Table A.3; [4, 5, 6, 8, 9, 10, 11]Solid solutions; [7]Estimated from the solubility of the Al-bearing analogues using $\Delta H_f^\circ = -215.2$ kcal/mol and $\Delta S_f^\circ = 4.8$ cal/mol/K (see text).
* For solids precipitating during the first 12 h, a higher solubility was assumed: gypsum: −4.30, syngenite: −6.45, portlandite: 23.25, tobermorite-II: −12.98, jennite: −11.18, ettringite: −42.84, Fe-ettringite: −47.16 and brucite: 17.29.

extended Debye–Hückel equation in Truesdell–Jones form with individual Kielland ion-size parameters $a_\gamma^\circ$ and common third parameter $b_\gamma$ [21]:

$$\log\gamma_j = \frac{-A_\gamma z_j^2\sqrt{I}}{1+B_\gamma a_\gamma^\circ\sqrt{I}} + b_\gamma I$$

where $z_j$ denotes the charge of species $j$, $I$ the effective molal ionic strength and $A_\gamma$ and $B_\gamma$ are P,T-dependent coefficients.

Thermodynamic data—with exception of the calcium sulphate data—are taken from the recent PSI-GEMS data set [21,22] supplemented with additional data for solids in cementitious materials as compiled in Table A.1. Additional solubility products for solids are recalculated as far as possible from experimental data published in the literature using Gibbs energy minimisation modelling [21]. In the few cases, where recalculation was not possible, the solubility products were rearranged using the auxiliary data from the respective source to refer to the aqueous species $Al(OH)_4^-$, $Fe(OH)_4^-$, $SiO(OH)_3^-$, and $OH^-$ in order to minimize the influence of the different auxiliary data sets.

### *A.1. C-S-H*

C-S-H phases are modelled using the solid solution model developed by Kulik and Kersten [37], where the C-S-H system is described as a system of two concurrent solid solution systems (cf. Fig. A.1):

(i) CSH-I solid solution system with the end-members $SiO_2$(am) and tobermorite (Tob-I: $Ca(OH)_2)_2(SiO_2)_{2.4}\cdot(H_2O)_2$), and
(ii) CSH-II solid solution system with the end-members jennite ($Ca(OH)_2)_{1.5}(SiO_2)_{0.9}\cdot(H_2O)_{0.9}$) and tobermorite (Tob-II: $Ca(OH)_2)_{1.5}(SiO_2)_{1.8}\cdot(H_2O)_{1.5}$).

Using the solid solution model [37] and based on the data of Greenberg and Chang [38], the respective solubility products are refitted using the PSI chemical thermodynamic database (Table A.1) for the best graphical fit to the observed pH and dissolved concentrations of Ca and Si (Fig. A.1). As already observed by Kulik and Kersten [37], at high C/S ratios the Si concentrations are slightly underestimated.

During the first hours and days of cement hydration, the morphology of the precipitating C-S-H phases changes markedly from the amorphous C-S-H via spongy to needle like C-S-H type [39]. It is not clear, however, whether also the C/S ratio of the solid and/or the solubility of the morphologically distinct C-S-H phases is changing. Using the solid solution model as described above which is based on data gained in a C-S-H system aged for several weeks [38], possibly underestimates the solubility of C-S-H during the first few hours of cement hydration.

### *A.2. Ettringite (AFt)*

Reported solubility products for ettringite range from log $K_{S0}=-43.13$ to $-46.43$ (cf. Table A.2). The experimental Al, S and Ca concentrations measured by Perkins and Palmer [40] were used to recalculate the solubility product of ettringite (cf. Table A.2), resulting in solubility products of $10^{-45.23}$ and $10^{-44.95}$ for the dissolution and precipitation experiments, respectively. The calculated mean value of $10^{-45.09\pm0.41}$ is in good agreement with other values reported in the literature.

Tricarboaluminate ($Ca_6Al_2(CO_3)_3(OH)_{12}\cdot 26H_2O$), the structural carbonate analogue of ettringite, is unstable relative to calcium monocarboaluminate and calcite [41]. Pöllmann and Kuzel [42] reported the extensive (but not complete) formation of solid solutions between the sulphate, hydroxide and carbonate ettringite end-members. The sulphate containing ettringite is significantly more stable than the OH or $CO_3$ substituted ettringites; however, a partial replacement of $SO_4^{2-}$ by $CO_3^{2-}$ and $OH^-$ is possible [42]. Thermodynamic data describing the solubility of $CO_3^{2-}$ substituted ettringite (tricarboaluminate) have been calculated using the solubility measurements given in Ref. [41] (cf. Table A.3).

For Fe-ettringite, which forms a solid solution with the Al-bearing ettringite [10,43], no experimentally derived

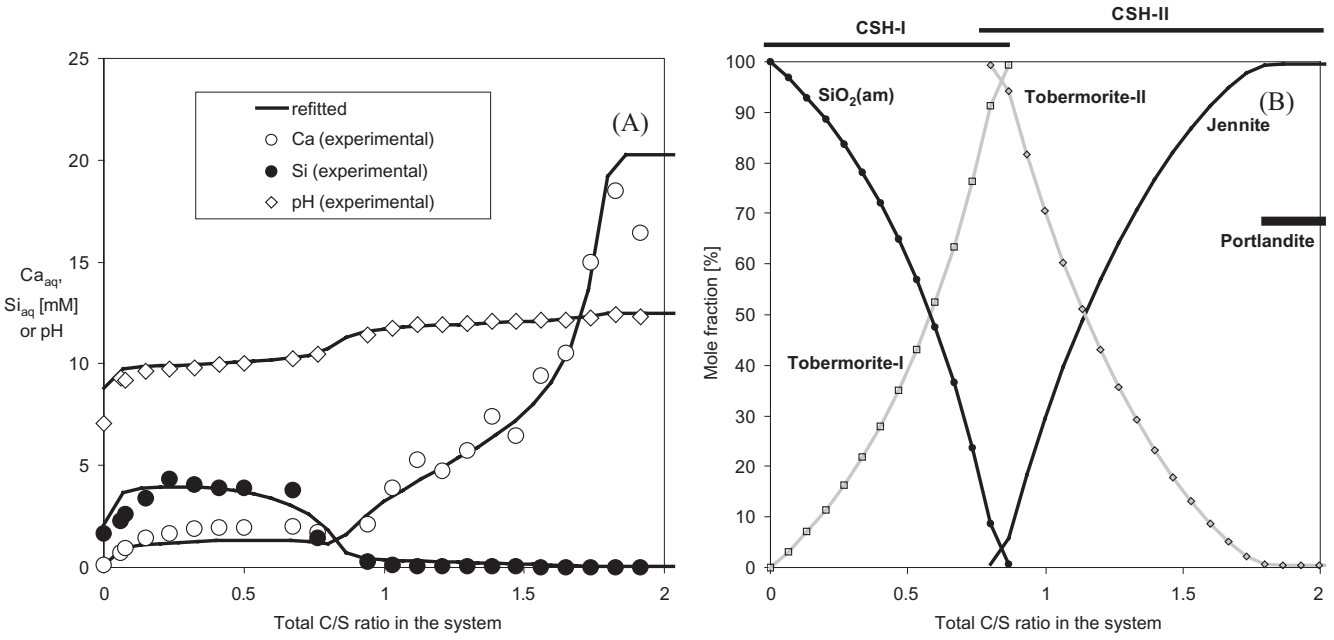


Fig. A.1. (A) Comparison of pH values, aqueous Ca and Si concentrations calculated with the C-S-H model proposed by Ref. [37] using the refitted solubility constants as given in Table A.1 with the experimental solubility results of Greenberg and Chang [38]. (B) Mole fractions of C-S-H solid solution endmembers with the refitted data (Table A.1). The presence of portlandite is indicated by a horizontal line (out of scale).

solubility data are available in the literature. Babushkin et al. [44] estimated between ferric and aluminium hydrates a constant difference in standard enthalpy and entropy of −215.2 kcal/mol and 4.8 cal/mol/K, respectively. This approach was applied to calculate the Gibbs free energies and the solubility product of Fe-ettringite and other iron-containing solids, resulting in a solubility product of $10^{-49.41}$ for Fe-ettringite $Ca_6Fe_2(SO_4)_3(OH)_{12}{\cdot}26H_2O$ (cf. Table A.1).

Thaumasite $Ca_3Si(OH)_6(SO_4)(CO_3)_{12}{\cdot}26H_2O$ has a structure similar to ettringite and is reported to form solid solution with ettringites. However, reliable solubility data for thaumasite were not available at the time this work was done.

### *A.3. AFm phases*

The AFm phases ($C_4(A,F)X_2{\cdot}yH_2O$, where $X$ denotes one formula unit of a single charged anion) occurring in cements are mineralogically and chemically complex. Its layer structure incorporates variable amounts of water as well as anions such as hydroxyl, sulphate, silicon, aluminate, or carbonate. Solid solutions between hydroxy- and sulphate-AFm and Al- and Fe-containing compounds are extensive [10,43,45,46], while solid solution formation between calcium monocarboaluminate, calcium hemicarboaluminate and hydroxy- or sulphate-AFm is very limited [45,47,48]. However, as only for the binary $C_2AH_8$–$C_4AH_x$ system a thermodynamic descriptions of the solid solutions has been published [49], the adequate description of the multicomponent AFm solid solution system present in cement is not yet possible. As a rough approximation, ideal solid solution behaviour has been assumed for all AFm phases, except for calcium hemi- and calcium monocarboaluminates, where no solid solution formation was considered.

For modelling the solubility of the metastable Ca-aluminates $C_2AH_8$ and $C_4AH_{13}$ (or $C_4AH_{19}$), the data recently fitted by Berner and Kulik [49] are used. These data are similar to the data reported by other authors (Table A.2), consider the formation of an ideal solid solution between the two endmembers and the solubility products can be used without any further fitting as they have been calculated using the same auxiliary database [21] as in this paper. For calcium monosulphoaluminate ($C_4A\bar{S}H_{12}$), a solubility product of $10^{-27.7}$ was fitted using the data measured by Jones [51] assuming the presence of $C_4A\bar{S}H_{12}$ and an ideal solution between the metastable endmembers $C_2AH_8$–$C_4AH_{13}$ [49]. Solid solution formation between sulphate and hydroxide-AFm have been observed mainly at the sulphate-rich end of the series [45,46], while at the hydroxide-AFm end—as in the experiments of Jones [51]—two distinct phases seem to predominate. The solubility products of calcium monosulphoaluminate determined from the data of Refs. [52] and [50] are somewhat lower (cf. Table A.3), which might be caused by the partial transformation of the metastable $C_4A\bar{S}H_{12}$ initially present to ettringite and $C_4AH_{13}$ in these experiments.

A solubility product of $10^{-20.49}$ for the AFm phase gehlenite hydrate or strätlingite $C_2ASH_8$ (cf. Table A.3) was calculated from the experimental data measured by [3,50].

Considerable uncertainty exists in the literature concerning the conditions for the existence of carboaluminate

Table A.2
Solubility products for solids in cementitious systems compiled from different literature sources

| AFt | | AFm | | | | | | | Hydrogarnets $CAH_{10}$ | | | Reference |
|---|---|---|---|---|---|---|---|---|---|---|---|---|
| Ettringite | $C_6F\bar{S}_3H_{32}$ | $C_4A\bar{S}H_{12}$ | $C_4F\bar{S}H_{12}$ | $C_4AH_{13}$ | $C_4AH_{19}$ | $C_4FH_{13}$ | $C_2AH_8$ | $C_2ASH_8$ | $C_3AH_6$ | $C_3FH_6$ | $CAH_{10}$ | |
| | | | | | −25.50 | | −13.75 | | −22.30 | | | [60] |
| | | | | | −25.50 | | −13.75 | | −22.30 | | | [61] |
| −44.00 | −49.78 | −28.19 | −34.05 | −27.92 | −27.94 | −33.78 | −13.26 | | −20.33 | −26.19 | −5.47 | [44] |
| | | | | −25.19 | | | −13.78 | | | | −7.59 | [62] |
| | | | | −25.19 | | | −13.78 | | −21.91 | | −7.58 | [63] |
| | | | | −25.16 | | | −13.99 | | −22.83 | | −7.49 | [53] |
| −43.13 | | −27.62 | | −27.49 | | | −13.04 | | −19.95 | | | [64] |
| −43.94 | | −29.25 | | | | | −13.75 | | −23.13 | | | [4] |
| −44.91 | | | | | | | | | −23.13 | | | [65] |
| −45.59 | | | | | | | | −20.57 | −21.25 | | | [3] |
| −44.44 | | | | | | | | | | | | [66] |
| −44.55 | | −29.43 | | | | | | | −22.54 | | | [67] |
| | | | | −25.4 | | | −13.73 | | −22.61 | | | [41] |
| −44.33 | | | | | | | | | −20.53 | | | [2] |
| −44.6 | | −29.43 | | | | | | | −22.54 | −30.36 | | [5][a] |
| −44.0 | | | | | −27.94 | | | | | | | [6] |
| −46.43 | | | | | | | | | | | | [68] |
| −45.54 | | −28.02 | | | | | | −20.56 | −21.20 | | | [7] |
| −45.13 | | | | | | | | | | | | [20] |
| −44.90 | | | | | | | | | | | | [40] |
| −45.00 | | −29.43 | | | | | | | | | | [8] |
| | | | | −25.56 | | | −13.56 | | −22.46 | | | [49] |

All solubility products refer to the solubility with respect to the species $Al(OH)_4^-$, $Fe(OH)_4^-$, $SiO(OH)_3^-$, $OH^-$, $H_2O$, $Ca^{2+}$or $SO_4^{2-}$. Where necessary, the solubility products have been rearranged using the respective auxiliary data set.

[a] Calculated by Ref. [5] using $G_f°$ values from Ref. [44] and various other sources.

phases. Damidot et al. [41] found that calcium hemicarboaluminate ($C_4A\bar{C}_{0.5}H_{12}$) is stable only over a limited range of $CO_2$ activities, while the calcium monocarboaluminate ($C_4A\bar{C}H_{11}$) is more stable and can exist also in the presence of $CaCO_3$. In the presence of carbonate, hydroxy—and sulphate—AFm phases readily transform to carboaluminate phases. The solubility products of calcium monocarboaluminate ($C_4A\bar{C}H_{11}$) and calcium hemicarboaluminate ($C_4A\bar{C}_{0.5}H_{12}$) have been calculated using the solubility measurements given in Refs. [41,12] and [52] (cf. Table A.3).

Again for the Fe-bearing analogues no experimentally derived solubility data have been found in the literature. Following the procedure outlined by Babushkin et al. [44], a constant difference in standard enthalpy and entropy of −215.2 kcal/mol and 4.8 cal/mol/K between ferric and aluminium hydrates was used to calculate the respective solubility products for $C_4FH_{13}$, $C_2FH_8$, $C_2FSH_8$, $C_4F\bar{S}H_{12}$, $C_4F\bar{C}H_{11}$ and $C_4F\bar{C}_{0.5}H_{12}$ (cf. Table A.1).

### A.4. Hydrogarnets

Hydrogarnets have structures related to grossular $C_3AS_3$. A solid solution series between $C_3AH_6$–$C_3FH_6$–$C_3AS_3$–$C_3FS_3$ has been reported, although the extent of Si substitutions at temperatures below 100 °C seems to be limited to one formula unit (siliceous hydrogarnet: $C_3ASH_4$) with a miscibility gap between hydrogarnet and the siliceous hydrogarnet [3,10]. Although hydrogarnet is a thermodynamically stable phase at ordinary temperatures, it is not found as a major hydration product in modern Portland cements even though minor quantities of poorly crystalline hydrogarnet may be present [10].

Several similar solubility products for hydrogarnet ($C_3AH_6$) are reported (cf. Table A.2) in the literature. For modelling, the solubility product fitted by Berner and Kulik [49] for $C_3AH_6$ was used. The solubility product of the Fe-analogue $C_3FH_6$ was calculated using the approach of Babushkin et al. [44] (cf. Table A.1). For siliceous hydrogarnet ($C_3ASH_4$) a solubility product of $10^{-31}$ was estimated from the data given in Bennet et al. [3] for the $C_3AH_6$–$C_3ASH_4$ system and from the observation of minor amounts of siliceous hydrogarnet in the experiments with strätlingite. However, the solubility product of siliceous hydrogarnet is based on very little and somewhat contradictory experimental evidence and is therefore not used in the present calculations. Further experimental data are needed to obtain a more reliable solubility product and for the description of this solid solution series.

### A.5. Other aluminate phases

While hydrogarnet is the thermodynamically stable phase, at low temperature (5 °C) metastable $Al(OH)_3$(am) and $CAH_{10}$ are formed. When temperature is increased, metastable $C_2AH_8$ and $C_4AH_{13}$ precipitate, while above 50 °C, $C_3AH_6$ is formed rapidly. The solubility products for the

Table A.3
Recalculated solubility products for different solid phases using solubility measurements from different literature sources

| Data source | Recalculated log $K_{S0}$ at 25 °C | Comments |
|---|---|---|
| Syngenite | $CaK_2(SO_4)_2{\cdot}H_2O \Leftrightarrow Ca^{2+}+2K^{+}+2SO_4^{2-}+H_2O$ | |
| [69] | −7.2 | Dissolution and precipitation; >20 data points |
| [70] | −7.4 | Only one experimental data point |
| [71] | **−7.2** | Experiments at 20 °C (log $K_{S0}$ at 20 °C = −7.21) |
| Ettringite | $Ca_6Al_2(SO_4)_3(OH)_{12}{\cdot}26H_2O \Leftrightarrow 6Ca^{2+}+2Al(OH)_4^{-}+3SO_4^{2-}+4OH^{-}+26H_2O$ | |
| [3] | −45.28 | Dissolution only; some $CO_2$ present |
| [40] | **−45.09** | Dissolution and precipitation; $CO_2$ and gypsum present |
| Tricarboaluminate | $3CaO{\cdot}Al_2O_3{\cdot}(CaCO_3)_3{\cdot}32H_2O \Leftrightarrow 6Ca^{2+}+2Al(OH)_4^{-}+3CO_3^{2-}+4OH^{-}+26H_2O$ | |
| [41] | **−41.3** | Some $CaCO_3$ precipitated |
| Gehlenite hydrate | $2CaO{\cdot}Al_2O_3{\cdot}SiO_2{\cdot}8H_2O \Leftrightarrow 2Ca^{2+}+2Al(OH)_4^{-}+Si(OH)_3^{-}+OH^{-}+2H_2O$ | |
| [3,50] | **−20.49** | Siliceous hydrogarnet present |
| Calcium monosulphoaluminate | $3CaO{\cdot}Al_2O_3{\cdot}CaSO_4{\cdot}12H_2O \Leftrightarrow 4Ca^{2+}+2Al(OH)_4^{-}+SO_4^{2-}+4OH^{-}+6H_2O$ | |
| [50] | −29.0 | Incongruent dissolution; ettringite precipitation |
| [52] | −29.8 | Incongruent dissolution; ettringite precipitation probable |
| [51] | **−27.70** | Fitted as $C_4ASH_{12\ and}$ ideal solid solution $C_2AH_8$–$C_4AH_{13}$ |
| Calcium monocarboaluminate | $3CaO{\cdot}Al_2O_3{\cdot}CaCO_3{\cdot}11H_2O \Leftrightarrow 4Ca^{2+}+2Al(OH)_4^{-}+CO_3^{2-}+4OH^{-}+5H_2O$ | |
| [52] | −32.58 | Some $CaCO_3$ precipitated; additional $CO_2$ present |
| [12] | −31.52 | Some $CaCO_3$ precipitated; additional $CO_2$ present |
| [41] | **−31.47** | Some $CaCO_3$ precipitated; additional $CO_2$ present |
| Calcium hemicarboaluminate | $3CaO{\cdot}Al_2O_3{\cdot}(CaCO_3)_{0.5}{\cdot}(Ca(OH)_2)_{0.5}{\cdot}11.5H_2O \Leftrightarrow 4Ca^{2+}+2Al(OH)_4^{-}+0.5CO_3^{2-}+5OH^{-}+5.5H_2O$ | |
| [41] | **−29.75** | $CaCO_3$ and additional $CO_2$ present |
| Siliceous hydrogarnet | $3CaO{\cdot}Al_2O_3{\cdot}SiO_2{\cdot}4H_2O+3H_2O \Leftrightarrow 3Ca^{2+}+2Al(OH)_4^{-}+SiO(OH)_3^{-}+3OH^{-}$ | |
| [3,50] | −31 | Estimation based on one experimental value; not used |
| OH−Hydrotalcite | $Mg_4Al_2(OH)_{14}{\cdot}3H_2O(cr) \Leftrightarrow 4Mg^{2+}+2Al(OH)_4^{-}+6OH^{-}+3H_2O$ | |
| [3,50] | **−56.02** | $Al(OH)_3$ precipitated |

All log K values refer to the formation of solids from the species $Al(OH)_4^{-}$, $Fe(OH)_4^{-}$, $SiO(OH)_3^{-}$, $OH^{-}$, $H_2O$, $Ca^{2+}$, $Mg^{2+}$, $SO_4^{2-}$, or $CO_3^{2-}$.

metastable $Al(OH)_3$(am) and $CAH_{10}$ are taken directly from the data calculated by Capmas and Ménétrier-Sorrentino [53].

### *A.6. Magnesium phases*

MgO present in the clinker phase will dissolve in the presence of water and precipitate in cementitious systems as brucite ($Mg(OH)_2$) or as hydrotalcite, depending on the chemical conditions. Hydrotalcites have a variable composition of the general formula $Mg_{1-x}(Al,Fe)_x(OH)_2{\cdot}[A^{n-}]_{x/n}{\cdot}mH_2O$, and a structure composed of positively charged brucite like layers intercalated with anions $[A^{n-}]$ and water molecules. The structure can accommodate a number of cations including Mn, Mg, Ni, Zn, Al, Fe, interlayer anions such as $OH^{-}$, $Cl^{-}$, $CO_3^{2-}$ and $SO_4^{2-}$ and varying amount of water [54–56].

Thermodynamic data for hydrotalcite are scarce due to its wide compositional variation. The solubility of OH-hydrotalcite ($Mg_4Al_2(OH)_{14}{\cdot}3H_2O$) aged for several days at 80 °C, has been determined experimentally by Refs. [50] and [3]. From these data a solubility product of $10^{-56.02}$ for $Mg_4Al_2(OH)_{14}{\cdot}3H_2O$(cr) was calculated using Gibbs energy minimisation modelling (cf. Table A.3). From the data recently determined for an amorphous precipitate ($Mg_4Al_2(OH)_{14}$(am)) after ~1 day [57], a solubility product of $10^{-49.2}$ can be calculated. Kvech and Edwards [57] observed also that in their solutions, the Al concentrations decreased further after roughly 100 h indicating some ageing processes and possibly the transformation to more crystalline hydrotalcite.

The solubility of $CO_3$-hydrotalcite ($Mg_4Al_2(OH)_{12}{\cdot}(CO_3){\cdot}2H_2O$) aged for 100 days was recently determined [58], resulting in a solubility product of $10^{-51.14}$ (cf. Table A.1). It is interesting to note that these thermodynamic data indicate that under conditions typical for Portland cements, i.e. a low partial pressure of $CO_2$, OH-hydrotalcite is more stable than $CO_3$-hydrotalcite.

## References

[1] U. Berner, A Thermodynamic Description of the Evolution of Pore Water Chemistry and Uranium Speciation During Degradation of Cement, (Report 90–12) PSI, Villigen, Switzerland, 1990.
[2] F.B. Neall, Modelling of the Near-field Chemistry of the SMA Repository at the Wellenberg Site, (Report 94–18) PSI, Villigen, Switzerland, 1994.

[3] D.G. Bennett, D. Read, M. Atkins, F.P. Glasser, A thermodynamic model for blended cements: II. Cement hydrate phases; thermodynamic values and modelling studies, J. Nucl. Mater. 190 (1992) 315–325.
[4] E.J. Reardon, Problems and approaches to the prediction of the chemical composition in cement/water systems, Waste Manage. 12 (1992) 221–239.
[5] J.H. Lee, D.M. Roy, B. Mann, D. Stahl, Integrated approach to modeling long-term durability of concrete engineered barriers in LLRW disposal facility, Mater. Res. Soc. Symp. Proc. 353 (1995) 881–889.
[6] C. Ayora, S. Chinchon, A. Aguado, F. Guirado, Weathering of iron sulfides and concrete alteration: thermodynamic model and observation in dams from Central Pyrenees, Spain, Cem. Concr. Res. 28 (1998) 1223–1235.
[7] V.A. Sinitsyn, D.A. Kulik, M.S. Khororivsky, I.K. Karpov, Prediction of solid-aqueous equilibria in cementitious systems using Gibbs energy minimization: I. Multiphase aqueous ideal solution models, Mater. Res. Soc. Symp. Proc. 506 (1998) 953–960.
[8] D. Rothstein, J.J. Thomas, B.J. Christensen, H.M. Jennings, Solubility behavior of Ca-, S-, Al-, and Si-bearing solid phases in Portland cement pore solutions as a function of hydration time, Cem. Concr. Res. 32 (2002) 1663–1671.
[9] H.W.W. Pollitt, A.W. Brown, The distribution of alkalis in Portland cement clinker, 5th ICCC, vol. 1, 1969, pp. 322–333.
[10] H.F.W. Taylor, Cement Chemistry, Thomas Telford Publishing, London, 1997.
[11] A. Franke, Bestimmung von Calciumoxid und Calciumhydroxid neben wasserfreiem und wasserhaltigem Calciumsilikat, Z. Anorg. Allg. Chem. 241 (1941) 180–184.
[12] T. Nishikawa, K. Sato, S. Ito, K. Suzuki, Thermal and chemical stability of AFm phase-isostructural group, 9th ICCC, vol. IV, 1992, pp. 437–442.
[13] W. Schwarz, Novel cement matrices by accelerated hydration of the ferrite phase in Portland cement via chemical activation: kinetics and cementitious properties, Adv. Cem. Based Mater. 2 (1995) 189–200.
[14] F.W. Locher, W. Richartz, S. Sprung, Erstarren von Zement: I. Reaktion und Gefügeentwicklung, Zem.-Kalk-Gips 29 (1976) 435–442.
[15] P. Gunkel, Die Zusammensetzung der flüssigen Phase erstarrender und erhärtender Zemente, Beton-Inf. 23 (1983) 3–8.
[16] P.G. Klepetsanis, E. Dalas, P.G. Koutsoukos, Role of temperature on the spontaneous precipitation of calcium dihydrate, Langmuir 15 (1999) 1534–1540.
[17] E.M. Gartner, F.J. Tang, S.J. Weiss, Saturation factors for calcium hydroxide and calcium sulfates in fresh Portland cement pastes, J. Am. Ceram. Soc. 68 (1985) 667–673.
[18] M. Zhang, Incorporation of oxyanionic B, Cr, Mo, and Se into hydrocalumite and ettringite: application to cementitious systems, PhD thesis. University of Waterloo, Waterloo, Canada, 2000.
[19] R.B. Perkins, C.D. Palmer, Solubility of chromate hydrocalumite ($3CaO{\cdot}Al_2O_3{\cdot}CaCrO_4{\cdot}nH2O$) 5–75 °C, Cem. Concr. Res. 31 (2001) 983–992.
[20] M. Ochs, B. Lothenbach, E. Giffaut, Uptake of oxo-anions by cements through solid-solution formation: experimental evidence and modelling, Radiochim Acta. 90 (2002) 639–646.
[21] D. Kulik, GEMS-PSI 2.0, PSI, Villigen, Switzerland, 2002, (available at http://les.web.psi.ch/Software/GEMS-PSI/).
[22] W. Hummel, U. Berner, E. Curti, F.J. Pearson, T. Thoenen, Nagra/PSI Chemical Thermodynamic Data Base 01/01, Universal Publishers/u-PUBLISH.com, USA, also published as Nagra Technical Report NTB 02–16, Nagra, Wettingen, Switzerland, 2002.
[23] S. Garrault, A. Nonat, Hydrated layer formation on tricalcium and dicalcium silicate surfaces: experimental study and numerical simulations, Langmuir 17 (2001) 8131–8138.
[24] A. Smith, T. Chotard, N. Gimet-Breart, D. Fargeot, Correlation between hydration mechanism and ultrasonic measurements in an aluminous cement: effect of setting time and temperature on the early hydration, J. Eur. Ceram. Soc. 22 (2002) 1947–1958.
[25] J.A. Dalziel, W.A. Gutteridge, The Influence of Pulverized-fuel Ash upon the Hydration Characteristics and Certain Physical Properties of a Portland Cement Paste, Tech. Rep., vol. 560, Cement and Concrete Association, Slough, 1986.
[26] L.J. Parrot, D.C. Killoh, Prediction of cement hydration, Br. Ceram. Proc. 35 (1984) 41–53.
[27] S. Swaddiwudhipong, D. Chen, M.H. Zhang, Simulation of the exothermic process of Portland cement, Adv. Cem. Res 14 (2002) 61–69.
[28] H.F.W. Taylor, A method for predicting alkali ion concentrations in cement pore solutions, Adv. Cem. Res 1 (1987) 5–17.
[29] S.-Y. Hong, F.P. Glasser, Alkali sorption by C-S-H and C-A-S-H gels: Part II. Role of alumina, Cem. Concr. Res. 32 (2002) 1101–1111.
[30] S.-Y. Hong, F.P. Glasser, Alkali binding in cement pastes: Part I. The C-S-H phase, Cem. Concr. Res. 29 (1999) 1893–1903.
[31] H.J.H. Brouwers, R.J. van Eijk, Alkali concentrations of pore solution in hydrating OPC, Cem. Concr. Res. 33 (2003) 191–196.
[32] H.-J. Kuzel, Initial hydration reactions and mechanisms of delayed ettringite formation in Portland cements, Cem. Concr. Compos. 18 (1996) 195–202.
[33] J.W. Johnson, E.H. Oelkers, H.C. Helgeson, SUPCRT92: a software package for calculating the standard molal thermodynamic properties of minerals, gases, aqueous species, and reactions from 1 to 5000 bar and 0 to 1000 °C, Comput. Geosci. 18 (1992) 899–947.
[34] D.A. Sverjensky, E.L. Shock, H.C. Helgeson, Prediction of the thermodynamic properties of aqueous metal complexes to 1000 °C and 5 kb, Geochim. Cosmochim. Acta 61 (1997) 1359–1412.
[35] E.L. Shock, D.C. Sassani, M. Willis, D.A. Sverjensky, Inorganic species in geologic fluids: correlations among standard molal thermodynamic properties of aqueous ions and hydroxide complexes, Geochim. Cosmochim. Acta 61 (1997) 907–950.
[36] E.L. Shock, An updated and augmented version (slop98.dat) of the original SUPCRT92 database (sprons92.dat) is available at http://epsc.wustl.edu/geopig/, 1998.
[37] D.A. Kulik, M. Kersten, Aqueous solubility diagrams for cementitious waste stabilization systems: II. End-member stoichiometries of ideal calcium silicates hydrate solid solutions, J. Am. Ceram. Soc. 84 (2001) 3017–3026.
[38] S.A. Greenberg, T.N. Chang, Investigation of the colloidal hydrated calcium silicates: II. Solubility relationships in the calcium oxide–silica–water system at 25°, J. Phys. Chem. 69 (1965) 182–188.
[39] L. Holzer, F. Winnefeld, B. Lothenbach, D. Zampini, The early cement hydration: a multi-method approach, 11th ICCC, 2003, pp. 236–248.
[40] R.B. Perkins, C.D. Palmer, Solubility of ettringite ($Ca_6[Al(OH)_6]_2(SO_4)_3{\cdot}26H_2O$) at 5–75 °C, Geochim. Cosmochim. Acta 63 (1999) 1969–1980.
[41] D. Damidot, S. Stronach, A. Kindness, M. Atkins, F.P. Glasser, Thermodynamic investigation of the $CaO–Al_2O_3–CaCO_3–H_2O$ closed system at 25 °C and the influence of $Na_2O$, Cem. Concr. Res. 24 (1994) 563–572.
[42] H. Pöllmann, H. Kuzel, Solid solution of ettringites, Cem. Concr. Res. 20 (1990) 941–947.
[43] A. Emanuelson, S. Hansen, Distribution of iron among ferrite hydrates, Cem. Concr. Res. 27 (1997) 1167–1177.
[44] V.I. Babushkin, G.M. Matveyev, O.P. Mchedlov-Petrossyan, Thermodynamics of Silicates, Springer-Verlag, Berlin, 1985.
[45] F.P. Glasser, A. Kindness, S.A. Stronach, Stability and solubility relationships in AFm phases: Part I. Chloride, sulfate and hydroxide, Cem. Concr. Res. 29 (1999) 861–866.
[46] H. Pöllmann, Solid solution in the system $3CaO{\cdot}Al_2O_3{\cdot}SO4{\cdot}aq–3CaO{\cdot}Al_2O_3{\cdot}Ca(OH)_4{\cdot}aq–H_2O$ at 25 °C, 45 °C, 60 °C, 80 °C, Neues Jahrb. Mineral. Abh. 161 (1989) 27–40.

[47] R. Fischer, H.-J. Kuzel, Reinvestigation of the system $C_4A{\cdot}nH_2O$–$C_4A{\cdot}CO_2{\cdot}nH_2O$, Cem. Concr. Res. 12 (1982) 517–526.
[48] H.-J. Kuzel, H. Pöllmann, Hydration of $C_3A$ in the presence of $Ca(OH)_2$, $CaSO_4{\cdot}2H_2O$ and $CaCO_3$, Cem. Concr. Res. 21 (1991) 885–895.
[49] U.R. Berner, D.A. Kulik, Ca-Al-hydrates: solid solutions? Geochim. Cosmochim. Acta 66 (2002) (A73-A73).
[50] M. Atkins, F.P. Glasser, A. Kindness, Cement hydrate phases: solubility at 25 °C, Cem. Concr. Res. 22 (1992) 241–246.
[51] F.E. Jones, The quaternary system $CaO–Al_2O_3–CaSO_4–H_2O$. Equilibria with crystalline $Al_2O_3{\cdot}3H_2O$, alumina gel, and solid solutions, J. Phys. Chem. 48 (1944) 311–356.
[52] F. Zhang, Z. Zhou, Z. Lou, Solubility product and stability of ettringite, 7th ICCC, vol. 2, 1980, pp. 88–93.
[53] A. Capmas, D. Ménétrier-Sorrentino, The effect of temperature on the hydration of calcium aluminate cement, UNITECR '89, 1989, pp. 1157–1170.
[54] L. Châtelet, J.Y. Bottero, J. Yvon, A. Bouchelaghem, Competition between monovalent and divalent anions for calcined and uncalcined hydrotalcite: anion exchange and adsorption sites, Colloids Surf., A Physicochem. Eng. Asp. 111 (1996) 167–175.
[55] J. Wang, A.G. Kalinichev, R.J. Kirkpatrick, X. Hou, Molecular modeling of the structure and energetics of hydrotalcite hydration, Chem. Mater. 13 (2001) 145–150.
[56] T. Sato, H. Fujita, T. Endo, M. Shimada, Synthesis of hydrotalcite like compounds and their physico-chemical properties, React. Solids 5 (1988) 219–228.
[57] S. Kvech, M. Edwards, Solubility controls on aluminum in drinking water at relatively low and high pH, Water Res. 36 (2002) 4356–4368.
[58] C.A. Johnson, F.P. Glasser, Hydrotalcite-like minerals $(M_2Al(OH)_6(CO_3)_{0.5}{\cdot}xH_2O$, where M=Mg, Zn, Co, Ni) in the environment: synthesis, characterisation and thermodynamic stability, Clay Clay Miner. 51 (2003) 1–8.
[59] D. Garvin, V.B. Parker, H.J. White, CODATA Thermodynamic Tables. Selections for Some Compounds of Calcium and Related Mixtures: A Prototype Set of Tables, Springer Verlag, Berlin, 1987.
[60] V.M. Nikushchenko, V.S. Khotimchenko, P.F. Rumyantsev, A.I. Kalinin, Determination of the standard free energies of formation of calcium hydroxyaluminates, Cem. Concr. Res. 3 (1973) 625–632.
[61] O.P. Mchedlov-Petrossyan, W.L. Tschernjawski, W.W. Ssawenkow, Über die Beständigkeit der Zementsteinmineralien in sulfat-und karbonathaltigen Wasserlösungen, Baustoffindustrie A19 (1976) 24–25.
[62] P. Barret, D. Bertrandie, Courbe d'instabilité minimale dans une solution métastable de CA, 7th ICCC, vol. V, 1980, pp. 134–139.
[63] P. Barret, D. Bertrandie, D. Beau, Calcium hydrocarboaluminate, carbonate, alumina gel and hydrated aluminates solubility diagram calculated in equilibrium with $CO_{2g}$ and with $Na^+_{aq}$ ions, Cem. Concr. Res. 13 (1983) 789–800.
[64] E.J. Reardon, An ion interaction model for the determination of chemical equilibria in cement/water systems, Cem. Concr. Res. 20 (1990) 175–192.
[65] C.J. Warren, E.J. Reardon, The solubility of ettringite at 25 °C, Cem. Concr. Res. 24 (1994) 1515–1524.
[66] D. Damidot, M. Atkins, A. Kindness, F.P. Glasser, Sulphate attack on concrete: limits of the AFt stability domain, Cem. Concr. Res. 22 (1992) 229–234.
[67] D. Damidot, F.P. Glasser, Thermodynamic investigation of the $CaO–Al_2O_3–CaSO_4–H_2O$ system at 25 °C and the influence of $Na_2O$, Cem. Concr. Res. 23 (1993) 221–238.
[68] S.C.B. Myneni, S.J. Traina, T.J. Logan, Ettringite solubility and geochemistry of the $Ca(OH)_2–Al_2(SO_4)_3–H_2O$ system at 1 atm pressure and 298 K, Chem. Geol. 148 (1998) 1–19.
[69] F.K. Cameron, J.F. Breazeale, Calcium sulphate in aqueous solutions of potassium and sodium sulphates, J. Phys. Chem. 8 (1904) 335–340.
[70] A.E. Hill, Ternary systems: XIX. Calcium sulfate, potassium sulfate and water, J. Am. Chem. Soc. 56 (1938) 1071–1078.
[71] E.M. Gartner, S. Sabio, J.P. Perez, Equilibria in the system calcium hydroxide–calcium sulphate–alkali sulphate–water at 5–30 °C, and their relevance to Portland cement hydration in the presence of superplasticizers, 11th ICCC, 2003, pp. 635–644.